

AnyPPG: An ECG-Guided PPG Foundation Model Trained on Over 100,000 Hours of Recordings for Holistic Health Profiling

Guangkun Nie*
School of Intelligence
Science and Technology,
Peking University
Beijing, China

Xiaocheng Fang*
School of Intelligence
Science and Technology,
Peking University
Beijing, China

Gongzheng Tang
National Institute of Health
Data Science, Peking
University
Beijing, China

Yujie Xiao
National Institute of Health
Data Science, Peking
University
Beijing, China

Jun Li
National Institute of Health
Data Science, Peking
University
Beijing, China

Bo Liu
School of Intelligence
Science and Technology,
Peking University
Beijing, China

Hongyan Li[†]
School of Intelligence
Science and Technology,
Peking University
Beijing, China

Shenda Hong[†]
National Institute of Health
Data Science, Peking
University
Beijing, China

Abstract

Photoplethysmography (PPG) is widely used as a non-invasive and accessible modality for continuous health monitoring. However, despite being a peripheral hemodynamic signal intrinsically coupled with systemic circulation, existing research has largely confined its scope to a narrow range of cardiovascular tasks, leaving a fundamental question underexplored: to what extent can PPG support holistic health profiling beyond traditional cardiovascular applications? To answer this question, we present AnyPPG, a foundation model-based framework designed to reveal the broader health-profiling potential of PPG. To ensure reliable performance for this investigation, AnyPPG is pretrained with ECG guidance on the most diverse PPG corpus with synchronized ECG to date, comprising over 100,000 hours of recordings from six large-scale data sources. This pretraining yields robust and physiologically grounded PPG representations that provide a reliable basis for subsequent analysis. Building upon this pretrained model, we conduct a systematic investigation into the association between PPG and holistic health through, to the best of our knowledge, the first PPG-based phenome-wide disease detection study, spanning 1,468 disease phenotypes in more than 15,000 subjects. Our evaluation demonstrates the effectiveness of AnyPPG: across eight clinical and wearable datasets covering 15 downstream tasks, it achieves the best performance in 13 tasks. More importantly, in the phenome-wide analysis, AnyPPG exhibits meaningful discriminative capability ($AUC \geq 0.70$) for 307 phenotypes across 16 distinct phecode chapters, including 230 non-circulatory conditions such as dementia, chronic kidney disease, hyperkalemia, and glaucoma, many of which have rarely been explored using PPG.

*These authors contributed equally to this research.

[†]Corresponding authors.

Permission to make digital or hard copies of all or part of this work for personal or classroom use is granted without fee provided that copies are not made or distributed for profit or commercial advantage and that copies bear this notice and the full citation on the first page. Copyrights for components of this work owned by others than the author(s) must be honored. Abstracting with credit is permitted. To copy otherwise, or republish, to post on servers or to redistribute to lists, requires prior specific permission and/or a fee. Request permissions from permissions@acm.org.

KDD '26, Jeju, Korea

© 2026 Copyright held by the owner/author(s). Publication rights licensed to ACM.
ACM ISBN 978-1-4503-XXXX-X/2026/08
<https://doi.org/XXXXXXXX.XXXXXXX>

Collectively, these findings indicate that easily acquired PPG signals encode rich health-related information extending well beyond conventional cardiovascular assessment, establishing a promising foundation for future research toward broader, scalable, and non-invasive PPG-based health applications. Code and model weights are available at <https://github.com/PKUDigitalHealth/AnyPPG>.

CCS Concepts

• **Applied computing** → **Health informatics**; • **Computing methodologies** → **Artificial intelligence**.

Keywords

Photoplethysmography, Foundation Models, Phenome-Wide Disease Detection, Holistic Health Profiling

ACM Reference Format:

Guangkun Nie, Xiaocheng Fang, Gongzheng Tang, Yujie Xiao, Jun Li, Bo Liu, Hongyan Li, and Shenda Hong. 2026. AnyPPG: An ECG-Guided PPG Foundation Model Trained on Over 100,000 Hours of Recordings for Holistic Health Profiling. In *Proceedings of (KDD '26)*. ACM, New York, NY, USA, 21 pages. <https://doi.org/XXXXXXXX.XXXXXXX>

1 Introduction

With the widespread adoption of wearable technologies, photoplethysmography (PPG) has emerged as a key modality for continuous, out-of-clinic health monitoring owing to its non-invasive nature and ease of integration [5, 65, 74]. PPG measures variations in peripheral blood volume, producing a waveform that reflects physiological attributes such as cardiac output, vascular compliance, and autonomic regulation [26, 46]. Recent advances in artificial intelligence have further enabled the effective utilization of PPG (AI-PPG) across a broad spectrum of applications, such as heart rate estimation [6, 48], cardiovascular disease screening [16, 50], and digital biomarker development [40, 45].

Despite substantial progress, existing research on PPG has remained largely focused on a narrow set of cardiovascular-related tasks, leaving its broader physiological relevance underexplored. PPG originates from the circulatory system, which is tightly coupled with organs and tissues throughout the body, suggesting that

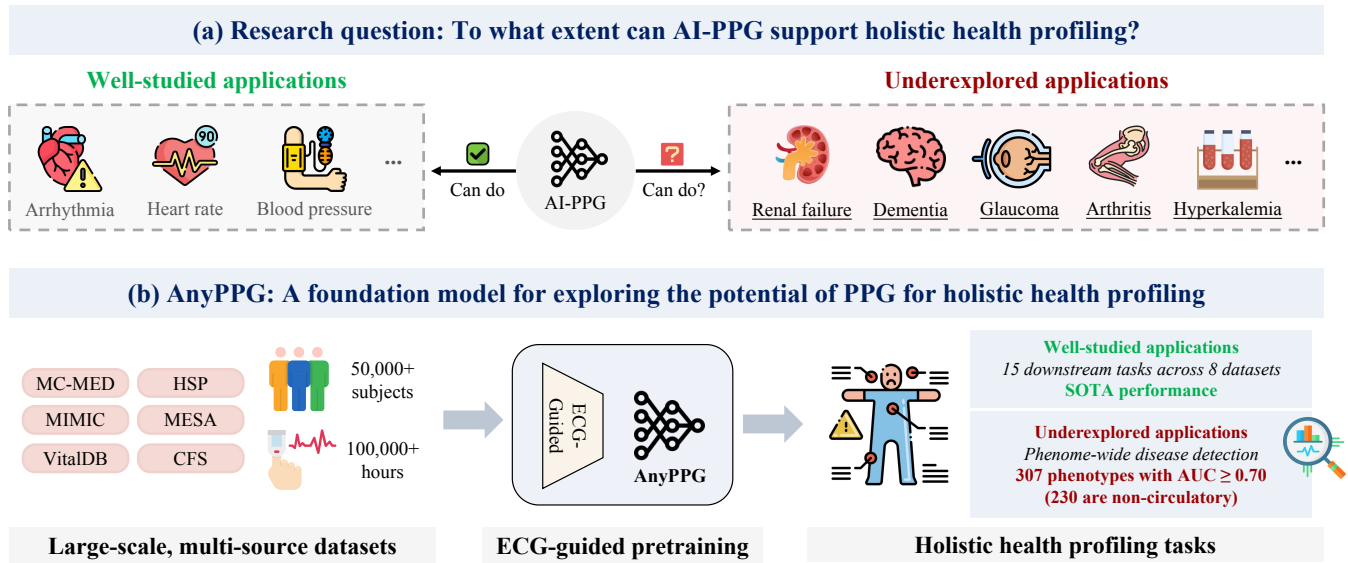


Figure 1: Research question and study overview of AnyPPG. (a) While PPG has been extensively studied for cardiovascular applications, its potential to support holistic health profiling across multi-organ conditions remains unclear. (b) To answer this question, we present AnyPPG, a foundation model-based framework designed to investigate the holistic health-profiling potential of PPG. AnyPPG leverages ECG-guided pretraining on the most diverse PPG corpus with synchronized ECG recordings to date, enabling the learning of physiologically grounded PPG representations and achieving SOTA performance on conventional PPG analysis tasks. Building upon this foundation, it further reveals broad associations between PPG and holistic health through a phenome-wide disease detection study spanning 1,468 phenotypes.

PPG signals may encode physiological information beyond conventional cardiovascular assessment. In contrast, recent studies on electrocardiography (ECG), which reflects the electrical activity of the heart and is closely linked to PPG, have demonstrated that cardiac electrical signals can support health assessment across a far broader clinical scope, ranging from the identification of kidney and liver diseases [2, 21, 35, 64] to full-spectrum analyses spanning diverse disease categories [24, 34]. This contrast raises a fundamental question: **to what extent can PPG support holistic health profiling beyond traditional cardiovascular applications?**

To bridge this research gap, we introduce AnyPPG, a foundation model-based framework designed to reveal the broader health-profiling potential of PPG. We organize this study under a two-stage paradigm. In the first stage, AnyPPG is pretrained on the most diverse PPG corpus with synchronized ECG to date, comprising over 100,000 hours of recordings from six large-scale data sources. This large-scale pretraining enables the model to learn robust and transferable PPG representations, providing a reliable foundation for subsequent investigation. Unlike prior approaches that rely solely on unimodal self-supervised learning [1, 10, 12, 51, 56], AnyPPG incorporates ECG as a source of cross-modal physiological supervision. Such supervision guides representation learning toward physiologically meaningful cardiovascular dynamics consistent with ECG while reducing sensitivity to non-physiological artifacts, yielding representations that are both robust and physiologically grounded. In the second stage, building upon this high-performing foundation model, we conduct a systematic investigation into the

association between PPG and holistic health through a large-scale PPG-based phenome-wide disease detection study spanning 1,468 disease phenotypes in more than 15,000 subjects, encompassing conditions far beyond well-studied cardiovascular diseases.

We begin by benchmarking AnyPPG on conventional PPG analysis tasks to assess representation quality, where it consistently achieves state-of-the-art (SOTA) performance compared with unimodal self-supervised methods, general-purpose time-series foundation models, and specialized PPG foundation models across eight independent downstream datasets, attaining the best results in 13 of 15 tasks. Building upon this validated foundation, the phenome-wide analysis further reveals meaningful discriminative capability across 16 distinct disease phenotype categories, with 307 phenotypes achieving an area under the curve (AUC) of at least 0.70. Strong performance is observed for 77 circulatory disorders, such as congestive heart failure (AUC = 0.84) and rheumatic heart valve disease (AUC = 0.81). Importantly, comparable discriminative capability is also demonstrated for 230 non-circulatory phenotypes, including dementia (AUC = 0.81), chronic renal failure (AUC = 0.75), hyperkalemia (AUC = 0.75), and glaucoma (AUC = 0.72), many of which have rarely been explored using PPG in prior research.

Specifically, our contributions are threefold:

- (1) We introduce AnyPPG, an ECG-guided PPG foundation model pretrained on the most diverse multi-source PPG corpus with synchronized ECG to date, yielding robust and transferable PPG representations.

- (2) We conduct a comprehensive evaluation of AnyPPG across eight diverse downstream datasets spanning both clinical and wearable settings, demonstrating consistent SOTA performance and achieving the best results in 13 of 15 tasks.
- (3) Building upon AnyPPG, we conduct, to the best of our knowledge, the first PPG-based phenome-wide disease detection study, spanning 1,468 disease phenotypes. This analysis provides quantitative evidence of broad associations between PPG and diverse disease phenotypes, many of which have rarely been explored in prior research, thereby revealing new directions for scalable and non-invasive PPG-based health assessment.

2 Related Work

2.1 PPG Foundation Models

Foundation models have demonstrated strong potential in healthcare and have been widely studied across domains such as computational pathology [37, 75], medical imaging [38, 67], and physiological signal analysis [33, 44, 68]. Through large-scale pretraining with supervised or self-supervised objectives, these models aim to learn transferable representations that generalize across diverse downstream tasks. In the context of PPG, existing foundation models primarily exploit intrinsic signal characteristics, including inter-individual variability, waveform morphology, susceptibility to noise and artifacts, and temporal predictability. Abbaspourazad et al. [1] and PaPaGEI-P [51] employ individual-level contrastive learning to encourage discrimination between PPG signals from different subjects, thereby capturing subject-specific representations. PaPaGEI-S [51] and PulsePPG [56] further incorporate waveform morphology by designing contrastive objectives based on physiological indices (e.g., stress-induced vascular response index) or motif-level similarity, enabling the extraction of physiologically meaningful features. Complementary to these approaches, SiamQuality [12] adopts a contrastive learning formulation that aligns representations of low- and high-quality PPG segments, improving robustness to signal degradation and noise. GPT-PPG [10], in contrast, explores generative pretraining inspired by autoregressive language models to learn representations from PPG time series.

To summarize, existing PPG foundation models primarily rely on unimodal self-supervised learning from PPG signals. In addition, their pretraining data are often derived from single-source [1, 10, 12, 56] or weakly heterogeneous datasets [51]. While effective at capturing specific signal characteristics, this paradigm may constrain the robustness and transferability of the learned representations. Given growing evidence that multimodal representation learning can improve representation quality and generalization [20, 52, 76, 80], incorporating multi-source data and cross-modal physiological supervision represents a promising direction for advancing PPG foundation models.

2.2 PPG-Based Healthcare Applications

As a physiological signal reflecting circulatory dynamics, PPG enables convenient and continuous monitoring of cardiovascular function and has been extensively studied in healthcare research. Existing PPG-based studies have predominantly focused

on cardiovascular-related applications, encompassing the estimation of physiological parameters such as heart rate [6, 48, 49], systolic/diastolic blood pressure [49, 58], oxygen saturation [30, 62], respiratory rate [60, 62], and blood glucose [26, 78], as well as the detection and screening of conditions including arrhythmia [50, 53], cardiac arrest [14, 61], hypertension [16, 41], and diabetes [4, 26]. Beyond these applications, PPG has also been explored in tasks such as emotion recognition [23, 25], stress analysis [42], and individual identification [71, 79], motivated by inter-individual variability in waveform morphology and its association with autonomic nervous system regulation. More recently, advances in deep learning have further extended PPG-based research to cross-modal signal synthesis, such as the generation of ECG [11, 17, 57, 77] and arterial blood pressure [7, 11], as well as the derivation of digital biomarkers related to cardiovascular health [40, 45].

Despite the expanding range of PPG-based applications, most existing studies remain centered on a narrow set of cardiovascular-related tasks, leaving the broader potential of PPG for holistic health profiling largely underexplored.

3 Methodology

In this section, we present AnyPPG, an ECG-guided PPG foundation model designed to learn robust and physiologically grounded representations from PPG signals. The pretrained model is subsequently used as a computational tool to investigate the extent to which PPG can support holistic health profiling.

3.1 Problem Formulation

Let $\mathcal{D} = \{(x_{p,i}, x_{e,i})\}_{i=1}^N$ denote a dataset of N synchronized PPG-ECG signal pairs, where $x_{p,i} \in \mathbb{R}^{L_p}$ and $x_{e,i} \in \mathbb{R}^{L_e}$ represent PPG and ECG segments of equal temporal duration. Our objective is to learn a parameterized PPG encoder $f_{\theta_p}(\cdot)$ that maps a raw PPG signal $x_{p,i}$ to a compact representation $z_{p,i} \in \mathbb{R}^{d_p}$, capturing transferable physiological dynamics for downstream tasks.

To this end, we introduce an auxiliary ECG encoder $f_{\theta_e}(\cdot)$ during pretraining and aim to align the representations of synchronized PPG-ECG pairs while separating mismatched pairs in the latent space. In this process, the ECG modality provides physiological supervision that guides the PPG encoder to capture hemodynamics consistent with cardiac electrical activity, thereby yielding robust and physiologically grounded PPG representations.

3.2 Pretraining Framework

To realize the cross-modal physiological alignment described above, AnyPPG adopts a dual-branch architecture composed of a PPG stream and an ECG stream. Each stream contains a modality-specific encoder followed by a projection head, enabling alignment of learned representations within a shared latent space. The overall framework is illustrated in Figure 2.

Modality-Specific Encoders. Each branch employs an encoder tailored to its input modality to extract latent physiological representations from raw waveforms. Given a synchronized pair $(x_{p,i}, x_{e,i})$, the encoders produce modality-specific latent features

$$z_{p,i} = f_{\theta_p}(x_{p,i}), \quad z_{e,i} = f_{\theta_e}(x_{e,i}), \quad (1)$$

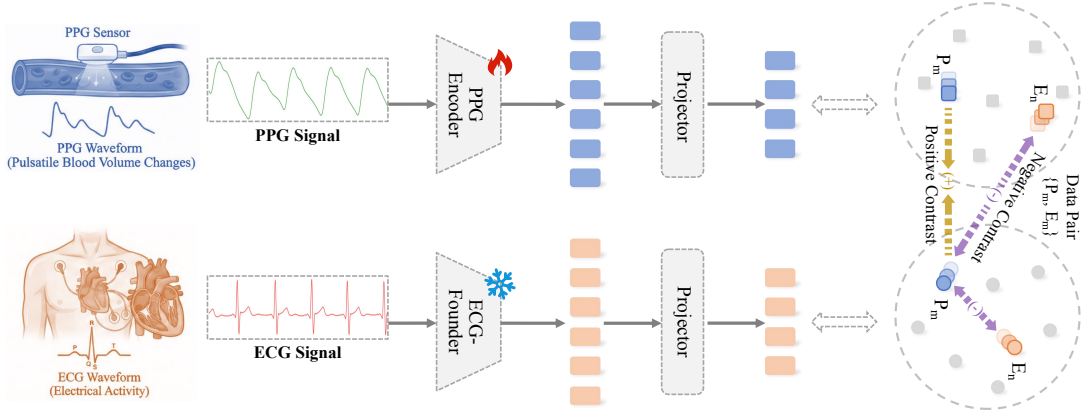


Figure 2: ECG-guided cross-modal pretraining of AnyPPG. AnyPPG learns robust and physiologically grounded PPG representations via contrastive alignment guided by ECGFounder [33], an ECG foundation model, in a shared latent space, aligning synchronized PPG-ECG pairs while separating mismatched ones.

where $z_{p,i}$ and $z_{e,i}$ denote the encoder-level representations of PPG and ECG signals, capturing complementary aspects of peripheral hemodynamics and cardiac electrical activity, respectively.

Projection Heads and Shared Latent Space. To enable cross-modal comparison, the encoder features are further mapped into a shared latent space through non-linear projection heads:

$$h_{p,i} = g_{\theta_p}(z_{p,i}), \quad h_{e,i} = g_{\theta_e}(z_{e,i}). \quad (2)$$

Here, $g_{\theta_p}(\cdot)$ and $g_{\theta_e}(\cdot)$ denote the projection heads (projectors) for the PPG and ECG branches, respectively, implemented as lightweight neural mappings placed on top of the encoders. The projected embeddings are further ℓ_2 -normalized to ensure scale-invariant similarity computation and stable contrastive optimization:

$$h_{p,i} \leftarrow \frac{h_{p,i}}{\|h_{p,i}\|_2}, \quad h_{e,i} \leftarrow \frac{h_{e,i}}{\|h_{e,i}\|_2}. \quad (3)$$

Cross-Modal Physiological Alignment. To leverage the intrinsic physiological coupling between cardiac electrical activity and peripheral hemodynamics, we adopt a CLIP-style contrastive learning objective [52] for cross-modal alignment. Given a mini-batch of B synchronized PPG-ECG pairs, the objective promotes correct cross-modal matching through a symmetric InfoNCE loss. Let $\text{sim}(u, v) = u^\top v$ denote the similarity between two ℓ_2 -normalized vectors. The PPG-to-ECG alignment loss is defined as

$$\mathcal{L}_{p \rightarrow e} = -\frac{1}{B} \sum_{i=1}^B \log \frac{\exp(\text{sim}(h_{p,i}, h_{e,i})/\tau)}{\sum_{j=1}^B \exp(\text{sim}(h_{p,i}, h_{e,j})/\tau)}, \quad (4)$$

and the ECG-to-PPG alignment loss $\mathcal{L}_{e \rightarrow p}$ is vice versa. The overall training objective is

$$\mathcal{L} = \frac{1}{2} (\mathcal{L}_{p \rightarrow e} + \mathcal{L}_{e \rightarrow p}), \quad (5)$$

where τ is a learnable temperature parameter that controls the sharpness of the similarity distribution. This contrastive objective increases similarity between synchronized PPG-ECG pairs while separating mismatched pairs, structuring the shared latent space according to physiologically consistent cardiovascular dynamics.

4 Experiments

4.1 Datasets and Splittings

Pretraining Datasets for AnyPPG. As summarized in Table 1, AnyPPG is pretrained on five large-scale publicly available datasets containing synchronized PPG and ECG recordings: MC-MED [29], PulseDB [73], the Multi-Ethnic Study of Atherosclerosis (MESA) [9], the Human Sleep Project (HSP) [66], and the Cleveland Family Study (CFS) [54]. PulseDB further aggregates waveform data from the MIMIC [27] and VitalDB [32] databases. Detailed dataset descriptions are provided in Appendix B.1. Across these sources, we curate 109,909 hours of synchronized waveform recordings from 58,796 subjects, yielding approximately 40 million paired 10-second PPG-ECG segments. For pretraining monitoring and evaluation, the paired segments are partitioned at the subject level into training, validation, and test subsets using an 8:1:1 split.

Downstream Datasets for Evaluation. Following the proposed two-stage study paradigm, we first evaluate the representation quality of AnyPPG on diverse downstream datasets spanning both clinical and portable or wearable environments. As summarized in Table 1, this evaluation includes eight PPG datasets: PPG-DaLiA [55], UCI-BP [28], BUT PPG [43], Gyro-Acc-PPG [31], WESAD [59], DeepBeat [69], Real-World PPG [63], and WenXinWuYang [72]. Together, these datasets form fifteen dataset-task pairs covering a broad spectrum of physiological analysis tasks. Detailed dataset descriptions are provided in Appendix B.2. For data splitting, when official train-test splits are unavailable, we perform subject-level splitting with an 8:2 ratio for datasets containing identifiable subjects and random sample-level splitting otherwise. For datasets with predefined splits, we follow the original experimental protocols.

Building on this representation-level validation, we further employ AnyPPG as a tool for large-scale phenome-wide disease phenotype detection to assess the broader health-profiling potential of PPG signals. This analysis is conducted on the MC-MED dataset. Although MC-MED is included in the pretraining corpus, the phenome-wide evaluation results are reported on a strictly disjoint cohort consisting of patients excluded from all pretraining subsets (e.g.,

Table 1: Datasets for pretraining and downstream evaluation. Task type: R (regression), B (binary), M- k (multiclass with k classes). Abbr.: HR, heart rate; SBP/DBP, systolic/diastolic blood pressure; RR, respiratory rate. * indicates complete exclusion from all pretraining splits.

Dataset	Used Modality	Task	Task Type	#Subj. (Segments)	Recording Hours
Phase I: Pretraining					
MC-MED [29]	PPG & ECG		–	49,916 (28,420,140)	78,945
PulseDB [73]	PPG & ECG		–	4,964 (4,596,304)	12,768
MESA [9]	PPG & ECG	PPG-ECG alignment	–	2,010 (2,860,924)	7,947
HSP [66]	PPG & ECG		–	1,584 (3,333,705)	9,260
CFS [54]	PPG & ECG		–	322 (355,870)	989
Total				58,796 (39,566,943)	109,909
Phase II: Evaluation					
PPG-DaLiA [55]	PPG	HR estimation	R	15 (12,943)	36
UCI-BP [28]	PPG	SBP estimation	R	N/A (261,563)	727
		DBP estimation	R	N/A (261,563)	727
		HR estimation	R	50 (3,840)	11
BUT PPG [43]	PPG	SBP estimation	R	50 (3,840)	11
		DBP estimation	R	50 (3,840)	11
		Signal quality assessment	B	50 (3,840)	11
Gyro-Acc-PPG [31]	PPG	HR estimation	R	24 (2,016)	6
DeepBeat [69]	PPG	Atrial fibrillation detection	B	N/A (536,399)	1,490
WESAD [59]	PPG	Emotion Recognition	M-4	15 (4,419)	12
Real-World PPG [63]	PPG	Biometric identification	B	35 (20,74)	3
WenXinWuYang [72]	PPG	HR estimation	R	N/A (10,035)	28
		RR estimation	R	N/A (10,035)	28
		Age estimation	R	N/A (10,035)	28
		Anomaly detection	B	N/A (10,035)	28
		Phenome-wide disease detection	M-1468	15,759 (359,900)	1,000

those without synchronized PPG-ECG recordings) and therefore never observed during pretraining, serving as a held-out test population independent of the pretraining training, validation, and test partitions. During evaluation, AnyPPG is fine-tuned using phenotype labels mapped from ICD-9/10 codes on the full set of subjects available in the pretraining cohort, and subsequently assessed on the strictly held-out cohort. For each hospitalization record, 20 PPG segments are randomly sampled from long-duration waveforms, and only phenotypes with more than 100 positive cases in the held-out test set are reported, resulting in a total of 1,468 phenotypes.

4.2 Data Preprocessing

For pretraining, continuous recordings are segmented into non-overlapping 10-second windows [30, 47]. Segments containing more than 25% invalid or motionless samples are discarded. The remaining segments are processed using band-pass filtering to suppress baseline drift and high-frequency noise: PPG signals are filtered within 0.5-8 Hz [15], while ECG signals are filtered within 0.5-40 Hz and further denoised using a 50 Hz notch filter to remove powerline interference [33]. ECG polarity inversion is automatically detected and corrected to ensure consistent waveform morphology [39], and ECG signal quality is assessed using established signal quality indices [81]. In contrast, no explicit signal quality filtering is applied to PPG segments, allowing the model to learn robustness to noise and motion artifacts. All retained segments are resampled to a uniform sampling rate of 125 Hz for PPG and 500 Hz for ECG, followed by z-score normalization along the temporal dimension.

For downstream evaluation, we follow the preprocessing protocols adopted in prior work [51].

4.3 Baselines and Implementation Details

Baseline Methods. We benchmark AnyPPG against a set of representative baselines spanning three complementary categories: unimodal PPG self-supervised methods, general-purpose time-series foundation models, and PPG-specific foundation models. (i) Unimodal self-supervised learning: To evaluate the contribution of cross-modal physiological supervision in AnyPPG, we train SimCLR [8] and BYOL [19] from scratch using only PPG signals from the same pretraining corpus; (ii) General-purpose time-series foundation models: We include MOMENT [18] and Chronos-2 [3] as representative general-purpose time-series foundation models. These models are evaluated as strong generic baselines to contextualize the performance of AnyPPG relative to broadly pretrained time-series representations; (iii) PPG-specific foundation models: PulsePPG [56] and PaPaGEI [51] are included as PPG-specific foundation models. These methods represent prior work most closely related to our setting and provide direct reference points for evaluating the performance of AnyPPG.

Implementation Details. For the implementation of AnyPPG, the PPG branch adopts Net1D [22], a one-dimensional convolutional architecture derived from ResNet and widely used in prior PPG foundation models such as PaPaGEI [51] and PulsePPG [56],

producing a 512-dimensional encoder representation (see Appendix A for details). The ECG branch leverages ECGFounder [33], an ECG foundation model pretrained on over 10 million recordings with supervised cardiovascular diagnosis labels, whose encoder outputs a 1024-dimensional representation. Each projection head is implemented as a lightweight multilayer perceptron composed of two linear layers with Batch Normalization and GELU activation in between. During pretraining, the ECGFounder encoder is frozen, while its projection head is updated jointly with the PPG branch using the symmetric InfoNCE loss. The learnable temperature parameter τ is initialized to 0.07.

Pretraining is conducted on four NVIDIA H20 GPUs with a per-GPU batch size of 2,560. Optimization uses AdamW [36] with an initial learning rate of 5×10^{-4} , a weight decay of 1×10^{-2} , and a cosine learning rate schedule. The model is trained for five epochs (77,160 optimization steps), including linear warm-up over the first 5,000 steps. Gradient clipping with a maximum norm of 1.0 is applied for training stability. Model checkpoints are saved every 500 steps, and the checkpoint achieving the lowest validation contrastive loss is selected for downstream evaluation. For SimCLR and BYOL baselines, we adopt identical pretraining settings to AnyPPG, including the same architecture, data, and optimization hyperparameters, ensuring a controlled comparison of learning objectives. For general-purpose time-series and PPG-specific foundation models, downstream evaluation is performed directly using their publicly released pretrained checkpoints.

4.4 Performance Evaluation

Evaluation Metrics. We evaluate both cross-modal representation alignment and downstream task performance using standard retrieval, regression, and classification metrics. For cross-modal alignment, retrieval quality is measured using Recall@k (R@1/5/10) and Mean Reciprocal Rank (MRR), capturing top-k matching accuracy and overall ranking consistency. All retrieval metrics are computed at the batch level and averaged across the evaluation set. For downstream tasks, Mean Absolute Error (MAE) is reported for regression, while AUC is used for classification. Additional metrics, including the Pearson correlation coefficient (r), accuracy, and F1-score, are provided in the appendix for a more comprehensive evaluation. In multi-class settings, AUC is computed using a one-vs-rest strategy and macro-averaged across classes.

Linear Probing and Fine-Tuning Strategy. To assess representation quality on physiological analysis tasks, we adopt a linear probing protocol following prior work [51, 56]. For all probing models, hyperparameters are selected via inner five-fold cross-validation on the training split, and final performance is reported on the held-out test set. For binary classification, logistic regression with the LBFGS solver is employed, with the inverse regularization strength searched over $C \in \{0.01, 0.1, 1, 10, 100\}$. For multi-class classification, we use a random forest classifier with grid-searched hyperparameters (number of estimators $\in \{100, 200\}$, maximum depth $\in \{10, 20\}$, and minimum samples split $\in \{2, 5\}$). For regression tasks, ridge regression is adopted, where the regularization parameter is chosen from $\alpha \in \{0.1, 1.0, 10.0, 100.0\}$ to minimize MAE. For phenotype-wide disease phenotype detection, the full AnyPPG model is fine-tuned end-to-end from the pretrained checkpoint.

Table 2: PPG-to-ECG retrieval performance of AnyPPG across datasets. Metrics are computed using a fixed retrieval pool of 512 paired samples and averaged across all batches.

Dataset	#Samples	R@1	R@5	R@10	MRR
MC-MED [29]	2,796,347	0.786	0.947	0.966	0.857
PulseDB [73]	510,408	0.608	0.921	0.975	0.742
MESA [9]	277,016	0.729	0.945	0.971	0.823
HSP [66]	333,059	0.796	0.978	0.994	0.876
CFS [54]	35,854	0.644	0.910	0.957	0.760
Sample-weighted Avg.	3,952,684	0.759	0.946	0.970	0.841
Macro Avg.		0.713	0.940	0.973	0.812

Fine-tuning is formulated as a multi-label classification problem jointly optimized across all available disease phenotypes.

5 Results

In this section, we present the experimental results in three progressive stages. First, Section 5.1 analyzes the cross-modal alignment achieved by the proposed pretraining strategy between PPG and ECG representations, demonstrating that AnyPPG learns physiologically meaningful PPG features consistent with ECG. Next, Section 5.2 evaluates the representation quality of AnyPPG across diverse downstream datasets, where it consistently achieves SOTA performance, confirming the robustness and generalizability of the learned representations. Finally, Section 5.3 extends the analysis to the large-scale phenome-wide setting, revealing broad associations between PPG signals and diverse disease phenotypes and highlighting the potential of PPG for holistic health profiling.

5.1 AnyPPG Effectively Aligns PPG and ECG Representations in a Shared Latent Space

Table 2 summarizes PPG-to-ECG retrieval performance on the test splits of the five pretraining datasets. Overall, AnyPPG demonstrates strong and consistent cross-modal alignment, achieving sample-weighted Recall@1, Recall@5, and Recall@10 of 0.759, 0.946, and 0.970, respectively, with a MRR of 0.841. These results reflect both high retrieval accuracy and stable ranking consistency. Notably, performance remains robust across datasets with diverse acquisition settings and population characteristics, suggesting that the learned representations capture physiologically meaningful structures that generalize beyond individual data sources.

5.2 AnyPPG Demonstrates Superior Performance Across Downstream Tasks

Tables 3 and 4 summarize downstream performance for regression and classification tasks, respectively. Overall, AnyPPG consistently outperforms all seven baseline models, achieving the best results on 13 of the 15 dataset-task pairs and ranking second on the remaining two, demonstrating strong and stable generalization across diverse downstream settings. Additional evaluation metrics and detailed results are provided in Appendix C.

Table 3: Linear-probing MAE for regression tasks. Best results are in red, second best are underlined. * indicates identical pretraining data to AnyPPG. Abbr.: HR, heart rate; SBP/DBP, systolic/diastolic blood pressure; RR, respiratory rate.

Dataset	Task	SimCLR* ICML'20	BYOL* NIPS'20	MOMENT ICML'24	Chronos-2 ArXiv'25	PulsePPG IMWUT'25	PaPaGEI-S ICLR'25	PaPaGEI-P ICLR'25	AnyPPG (Ours)
PPG-DaLiA	HR	<u>9.37</u> _[9.01, 9.74]	9.51 _[9.17, 9.87]	10.43 _[10.05, 10.79]	10.50 _[10.14, 10.86]	10.79 _[10.41, 11.20]	12.88 _[12.50, 13.25]	11.69 _[11.31, 12.04]	9.27 _[8.90, 9.62]
	HR	7.63 _[6.13, 9.19]	9.23 _[7.52, 11.24]	7.35 _[6.00, 8.88]	<u>7.05</u> _[5.92, 8.27]	7.55 _[5.98, 9.07]	8.92 _[7.31, 10.51]	11.16 _[8.28, 14.58]	5.47 _[4.39, 6.72]
BUT PPG	SBP	17.15 _[14.23, 20.28]	17.71 _[14.73, 20.73]	14.71 _[12.07, 17.51]	14.55 _[12.40, 17.09]	16.87 _[14.41, 19.64]	<u>14.50</u> _[11.59, 17.58]	25.76 _[17.06, 36.51]	13.31 _[11.03, 15.68]
	DBP	11.15 _[9.94, 12.51]	12.47 _[10.91, 14.28]	10.75 _[9.46, 12.05]	10.24 _[9.15, 11.35]	11.32 _[10.00, 12.77]	11.02 _[9.73, 12.24]	9.30 _[7.92, 10.58]	<u>9.62</u> _[8.41, 10.79]
Gyro-Acc-PPG	HR	<u>11.38</u> _[10.32, 12.55]	11.45 _[10.47, 12.55]	13.34 _[12.09, 14.57]	13.10 _[12.16, 14.04]	12.56 _[11.27, 13.72]	17.20 _[15.84, 18.50]	14.63 _[13.46, 15.76]	10.82 _[9.78, 11.85]
UCI-BP	SBP	<u>15.70</u> _[15.59, 15.80]	15.95 _[15.84, 16.06]	16.57 _[16.46, 16.68]	17.05 _[16.94, 17.16]	16.54 _[16.44, 16.65]	17.56 _[17.45, 17.68]	16.80 _[16.69, 16.92]	15.62 _[15.51, 15.72]
	DBP	7.14 _[7.09, 7.19]	<u>7.31</u> _[7.26, 7.37]	7.53 _[7.47, 7.58]	7.69 _[7.63, 7.74]	7.57 _[7.51, 7.63]	7.88 _[7.82, 7.93]	7.68 _[7.63, 7.73]	7.14 _[7.09, 7.19]
WenXinWuYang	HR	7.14 _[6.81, 7.47]	<u>7.07</u> _[6.76, 7.39]	7.14 _[6.80, 7.48]	7.22 _[6.92, 7.55]	7.28 _[6.95, 7.66]	9.47 _[9.13, 9.82]	7.99 _[7.63, 8.35]	6.83 _[6.50, 7.18]
	RR	2.33 _[2.24, 2.42]	<u>2.32</u> _[2.24, 2.40]	2.36 _[2.24, 2.42]	<u>2.32</u> _[2.23, 2.40]	2.36 _[2.27, 2.44]	2.33 _[2.24, 2.42]	2.33 _[2.25, 2.41]	2.30 _[2.22, 2.39]
	Age	<u>6.09</u> _[5.91, 6.29]	6.08 _[5.90, 6.27]	6.19 _[5.99, 6.37]	6.19 _[6.01, 6.37]	6.27 _[6.05, 6.46]	6.47 _[6.29, 6.67]	6.33 _[6.15, 6.55]	6.08 _[5.89, 6.26]

Table 4: Linear-probing AUC for classification tasks. Best results are in red, second best are underlined. * indicates identical pretraining data to AnyPPG.

Dataset	Task	SimCLR* ICML'20	BYOL* NIPS'20	MOMENT ICML'24	Chronos-2 ArXiv'25	PulsePPG IMWUT'25	PaPaGEI-S ICLR'25	PaPaGEI-P ICLR'25	AnyPPG (Ours)
WESAD	Emotion recognition	0.77 _[0.75, 0.79]	0.74 _[0.72, 0.76]	0.71 _[0.69, 0.73]	0.74 _[0.72, 0.76]	0.73 _[0.71, 0.75]	0.67 _[0.65, 0.69]	0.71 _[0.69, 0.73]	<u>0.76</u> _[0.74, 0.78]
DeepBeat	Atrial fibrillation detection	<u>0.68</u> _[0.67, 0.69]	0.64 _[0.63, 0.65]	0.60 _[0.59, 0.61]	0.66 _[0.65, 0.67]	0.60 _[0.59, 0.60]	0.57 _[0.56, 0.58]	0.59 _[0.58, 0.59]	0.69 _[0.68, 0.70]
BUT PPG	Signal quality assessment	<u>0.73</u> _[0.66, 0.79]	0.79 _[0.74, 0.84]	0.77 _[0.72, 0.81]	0.79 _[0.74, 0.84]	0.76 _[0.71, 0.81]	0.67 _[0.61, 0.73]	0.69 _[0.62, 0.76]	0.79 _[0.73, 0.84]
Real-World PPG	Biometric identification	1.00 _[1.00, 1.00]	1.00 _[1.00, 1.00]	0.96 _[0.96, 0.97]	0.88 _[0.87, 0.90]	1.00 _[1.00, 1.00]	0.88 _[0.87, 0.89]	<u>0.99</u> _[0.99, 1.00]	1.00 _[1.00, 1.00]
WenXinWuYang	Anomaly detection	0.67 _[0.64, 0.70]	0.67 _[0.64, 0.70]	0.68 _[0.65, 0.71]	<u>0.69</u> _[0.67, 0.72]	<u>0.69</u> _[0.66, 0.72]	0.57 _[0.55, 0.61]	0.68 _[0.65, 0.71]	0.72 _[0.69, 0.75]

Compared with unimodal self-supervised baselines (SimCLR and BYOL), AnyPPG yields notably larger improvements on datasets collected from real-world wearable and mobile devices, including BUT PPG and Gyro-Acc-PPG. On these datasets, AnyPPG achieves average performance gains of approximately 15.4% and 18.8%, respectively. Given that these data are characterized by motion artifacts and variable signal quality, the observed improvements suggest that cross-modal ECG supervision helps the model learn representations that are more robust under challenging acquisition conditions than those learned with unimodal self-supervised objectives.

When further compared with general-purpose time-series foundation models pretrained on large-scale, multi-domain temporal data (MOMENT and Chronos-2), AnyPPG achieves the best performance on all 15 tasks. While these models exhibit competitive results in specific areas, such as signal quality assessment on the BUT PPG dataset, AnyPPG consistently outperforms them across the board. This disparity suggests that generic temporal representations may fail to fully capture the intricate physiological characteristics inherent to PPG signals. In contrast, the physiologically grounded

cross-modal alignment in AnyPPG facilitates more effective transfer to PPG-centric downstream applications.

Finally, compared with existing PPG-specific foundation models, AnyPPG achieves superior performance on 14 of the 15 tasks, underscoring the benefit of combining cross-modal physiological supervision with large-scale, multi-source pretraining. Notably, general self-supervised frameworks (SimCLR and BYOL), when trained on the same pretraining corpus as AnyPPG, also outperform PPG-specific models on a subset of tasks, suggesting that the scale and diversity of pretraining data play a critical role in determining representation quality. Collectively, these findings indicate that AnyPPG provides highly effective and generalizable representations for PPG analysis across diverse downstream settings.

5.3 AnyPPG Reveals the Potential of PPG for Holistic Health Profiling

In the phenome-wide disease detection study comprising a total of 1,468 disease phenotypes, AnyPPG demonstrates discriminative capacity across a broad spectrum of diseases rather than being limited to cardiovascular conditions. This global discriminative

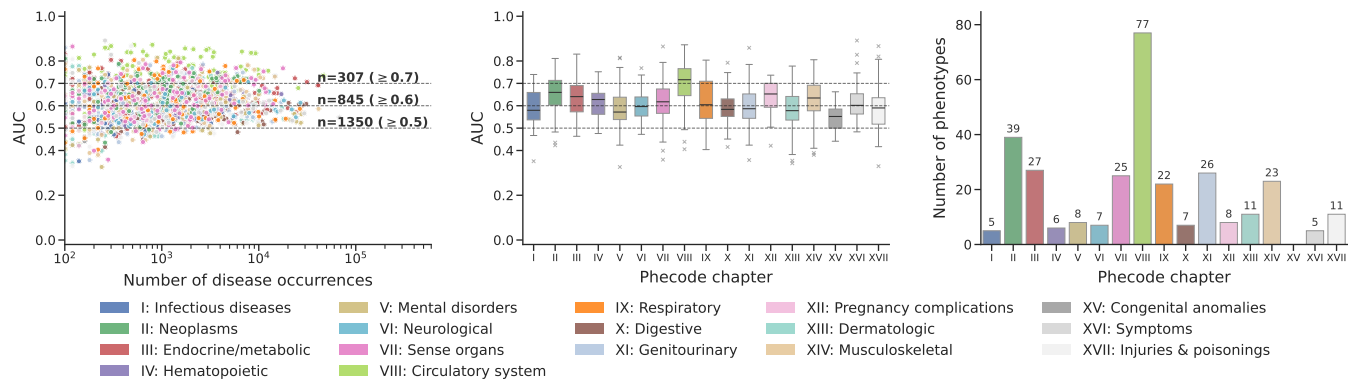


Figure 3: Phenome-wide disease detection performance of AnyPPG. Left: Distribution of AUC scores for 1,468 disease phenotypes. Middle: Chapter-level AUC performance distribution. Right: Count of high-performing phenotypes (AUC \geq 0.70) across different phecode chapters.

capacity is first reflected at the phenotype level (left panel of Figure 3), where 307 of the 1,468 evaluated phenotypes achieve an AUC of at least 0.70, and 845 and 1,350 phenotypes exceed AUC thresholds of 0.60 and 0.50, respectively, indicating that the vast majority of disease phenotypes exhibit detectable patterns with at least partial discriminative ability based solely on PPG signals. Consistent with this phenotype-level observation, chapter-level aggregation (middle panel) shows mean AUC values above the 0.50 baseline across all phecode chapters, with several non-circulatory categories, such as endocrine/metabolic disorders and hematopoietic diseases, surpassing 0.60. Importantly, the right panel reveals that high-performing phenotypes are not confined to circulatory diseases but are broadly distributed across organ systems. Chapters including neoplasms, endocrine/metabolic disorders, sense organs, respiratory, genitourinary, and musculoskeletal conditions each contain more than 20 phenotypes with AUC values above 0.70.

To further characterize high-performing phenotypes, we examined the top 60 conditions ranked by AUC (see Appendix Figure A1 for the full list). All Top-60 phenotypes achieve AUC values of at least 0.78, indicating consistently strong discriminative performance. Circulatory diseases account for 31 of the 60 phenotypes and can be broadly grouped into three categories: (i) cardiac pump dysfunction, such as heart failure; (ii) structural and valvular abnormalities, including mitral or tricuspid valve disorders; and (iii) electrophysiological conduction disturbances, such as atrial fibrillation and left bundle branch block. Importantly, strong performance extends well beyond cardiovascular conditions. The remaining 29 phenotypes arise from ten non-circulatory chapters, demonstrating the broad physiological relevance of PPG-derived representations. Representative examples include diabetic retinopathy (AUC = 0.83) and amyloidosis (AUC = 0.81) within endocrine and metabolic disorders, dementia-related phenotypes (AUC = 0.81) in the neurological chapter, and corneal dystrophy (AUC = 0.86) and wet macular degeneration (AUC = 0.79) in sense organs, many of which have rarely been investigated using PPG in prior work. Moreover, the Top-60 results represent only a small portion of the total 307 discriminative phenotypes (detailed in Appendix D). Meaningful discriminative capability is also observed across numerous additional clinically

meaningful non-circulatory conditions, such as Parkinson’s disease (AUC = 0.77), hyperkalemia (AUC = 0.75), chronic renal failure (AUC = 0.75), and anemia of chronic disease (AUC = 0.72).

Collectively, these findings suggest that PPG reflects integrated physiological alterations across a broad spectrum of conditions, such as metabolic, neurological, and hematological disorders [13, 70], supporting its potential for holistic health profiling.

6 Limitations and Ethical Considerations

This study has several limitations. First, the phenome-wide evaluation was conducted in a single clinical cohort, and the observed associations may therefore reflect cohort-specific characteristics. External validation across additional medical centers and more diverse populations is needed to assess robustness and generalizability. Moreover, although the phenome-wide analysis identifies disease phenotypes discriminable from PPG-derived representations, these findings should be interpreted as quantifying broad associations rather than establishing causal relationships.

All datasets used in this study, except for the WenXinWuYang dataset, are publicly available, and the requirements for Institutional Review Board approval and informed consent were waived accordingly. The proprietary WenXinWuYang dataset was collected using consumer-grade devices and contains only de-identified physiological signals and basic health-related metrics. Its use was reviewed and approved by the Peking University Medical Ethics Committee (Approval No.: IRB00001052-23071).

7 Conclusion

In this work, we introduced AnyPPG, an ECG-guided PPG foundation model that achieves state-of-the-art performance in PPG analysis and enables investigation of the extent to which PPG can support holistic health profiling beyond traditional cardiovascular tasks. Through large-scale phenome-wide analysis on over 15,000 subjects, we show that PPG representations learned by AnyPPG capture clinically relevant information across both circulatory and non-circulatory conditions. These findings provide a foundation for future research exploring the broader role of PPG in holistic health assessment.

GenAI Disclosure

During this research and manuscript preparation, we use large language models (LLMs) for auxiliary tasks such as generating short scripts during coding and assisting with text translation and language polishing. All core ideas, research methodologies, and academic contributions are conceived and developed independently by the authors, with the role of LLMs limited to improving the fluency and readability of the presentation.

References

- [1] Salar Abbaspourazad, Oussama Elachqar, Andrew C Miller, Saba Emrani, Udhayakumar Nallasamy, and Ian Shapiro. 2023. Large-scale training of foundation models for wearable biosignals. *arXiv preprint arXiv:2312.05409* (2023).
- [2] Juan Miguel Lopez Alcaraz, Wilhelm Haverkamp, and Nils Strothoff. 2025. Electrocardiogram-based diagnosis of liver diseases: an externally validated and explainable machine learning approach. *EClinicalMedicine* 84 (2025).
- [3] Abdul Fatir Ansari, Oleksandr Shchur, Jaris Küken, Andreas Auer, Boran Han, Pedro Mercado, Syama Sundar Rangapuram, Huibin Shen, Lorenzo Stella, Xiyuan Zhang, et al. 2025. Chronos-2: From univariate to universal forecasting. *arXiv preprint arXiv:2510.15821* (2025).
- [4] Robert Avram, Jeffrey E Olgin, Peter Kuhar, J Weston Hughes, Gregory M Marcus, Mark J Pletcher, Kirstin Aschbacher, and Geoffrey H Tison. 2020. A digital biomarker of diabetes from smartphone-based vascular signals. *Nature medicine* 26, 10 (2020), 1576–1582.
- [5] Karim Bayoumy, Mohammed Gaber, Abdallah Elshafeey, Omar Mhaimeed, Elizabeth H Dineen, Françoise A Marvel, Seth S Martin, Evan D Muse, Mintu P Turakhia, Khaldoun G Tarakji, et al. 2021. Smart wearable devices in cardiovascular care: where we are and how to move forward. *Nature Reviews Cardiology* 18, 8 (2021), 581–599.
- [6] Brinnae Bent, Benjamin A Goldstein, Warren A Kibbe, and Jessilyn P Dunn. 2020. Investigating sources of inaccuracy in wearable optical heart rate sensors. *NPJ digital medicine* 3, 1 (2020), 18.
- [7] Cheng Bian, Xiaoyu Li, Qi Bi, Guangpu Zhu, Jiegeng Lyu, Weile Zhang, Yelei Li, and Zijiang Zeng. 2024. Constraint latent space matters: an anti-anomalous waveform transformation solution from photoplethysmography to arterial blood pressure. In *Proceedings of the AAAI Conference on Artificial Intelligence*, Vol. 38. 11087–11095.
- [8] Ting Chen, Simon Kornblith, Mohammad Norouzi, and Geoffrey Hinton. 2020. A simple framework for contrastive learning of visual representations. In *International conference on machine learning*. PmlR, 1597–1607.
- [9] Xiaoli Chen, Rui Wang, Phyllis Zee, Pamela L Lutsey, Sogol Javaheri, Carmela Alcántara, Chandra L Jackson, Michelle A Williams, and Susan Redline. 2015. Racial/ethnic differences in sleep disturbances: the Multi-Ethnic Study of Atherosclerosis (MESA). *Sleep* 38, 6 (2015), 877–888.
- [10] Zhaoliang Chen, Cheng Ding, Saurabh Kataria, Runze Yan, Minxiao Wang, Randall Lee, and Xiao Hu. 2025. GPT-PPG: a GPT-based foundation model for photoplethysmography signals. *Physiological Measurement* 46, 5 (2025), 055004.
- [11] Zehua Chen, Yuyang Miao, Liyuan Wang, Luyun Fan, Danilo P Mandic, and Jun Zhu. 2025. Versatile cardiovascular signal generation with a unified diffusion transformer. *Nature Machine Intelligence* (2025), 1–14.
- [12] Cheng Ding, Zhicheng Guo, Zhaoliang Chen, Randall J Lee, Cynthia Rudin, and Xiao Hu. 2024. SiamQuality: a ConvNet-based foundation model for photoplethysmography signals. *Physiological Measurement* 45, 8 (2024), 085004.
- [13] Elia J Duh, Jennifer K Sun, and Alan W Stitt. 2017. Diabetic retinopathy: current understanding, mechanisms, and treatment strategies. *JCI insight* 2, 14 (2017), e93751.
- [14] Roos Edgar, Niels TB Scholte, Kambiz Ebrahimkheil, Marc A Brouwer, Rypko J Beukema, Masih Mafi-Rad, Kevin Vernooij, Sing-Chien Yap, Eelko Ronner, Nicolas van Mieghem, et al. 2024. Automated cardiac arrest detection using a photoplethysmography wristband: algorithm development and validation in patients with induced circulatory arrest in the DETECT-1 study. *The Lancet Digital Health* 6, 3 (2024), e201–e210.
- [15] Mohamed Elgendi. 2012. On the analysis of fingertip photoplethysmogram signals. *Current cardiology reviews* 8, 1 (2012), 14–25.
- [16] Mohamed Elgendi, Richard Fletcher, Yongbo Liang, Newton Howard, Nigel H Lovell, Derek Abbott, Kenneth Lim, and Rabab Ward. 2019. The use of photoplethysmography for assessing hypertension. *NPJ digital medicine* 2, 1 (2019), 60.
- [17] Xiaocheng Fang, Jiarui Jin, Haoyu Wang, Che Liu, Jieyi Cai, Guangkun Nie, Jun Li, Hongyan Li, and Shenda Hong. 2025. PPGFlowECG: Latent Rectified Flow with Cross-Modal Encoding for PPG-Guided ECG Generation and Cardiovascular Disease Detection. *arXiv preprint arXiv:2509.19774* (2025).
- [18] Mononito Goswami, Konrad Szafer, Arjun Choudhry, Yifu Cai, Shuo Li, and Artur Dubrawski. 2024. Moment: A family of open time-series foundation models. *arXiv preprint arXiv:2402.03885* (2024).
- [19] Jean-Bastien Grill, Florian Strub, Florent Alché, Corentin Tallec, Pierre Richemond, Elena Buchatskaya, Carl Doersch, Bernardo Avila Pires, Zhaohan Guo, Mohammad Gheshlaghi Azar, et al. 2020. Bootstrap your own latent—a new approach to self-supervised learning. *Advances in neural information processing systems* 33 (2020), 21271–21284.
- [20] Zhicheng Guo, Cheng Ding, Duc H Do, Amit Shah, Randall J Lee, Xiao Hu, and Cynthia Rudin. 2023. SiamAF: learning shared information from ECG and PPG signals for robust atrial fibrillation detection. *arXiv preprint arXiv:2310.09203* (2023).
- [21] Lauri Holmstrom, Matthew Christensen, Neal Yuan, J Weston Hughes, John Theurer, Melvin Jujjavarapu, Pedram Fatehi, Alan Kwan, Roopinder K Sandhu, Joseph Ebinger, et al. 2023. Deep learning-based electrocardiographic screening for chronic kidney disease. *Communications Medicine* 3, 1 (2023), 73.
- [22] Shenda Hong, Yanbo Xu, Alind Khare, Satria Priambada, Kevin Maher, Alaa Aljiffry, Jimeng Sun, and Alexey Tumanov. 2020. HOLMES: Health OnLine Model Ensemble Serving for Deep Learning Models in Intensive Care Units. In *Proceedings of the 26th ACM SIGKDD International Conference on Knowledge Discovery & Data Mining*. 1614–1624.
- [23] Tuck-Voon How, Robin EA Green, and Alex Mihailidis. 2023. Towards PPG-based anger detection for emotion regulation. *Journal of NeuroEngineering and Rehabilitation* 20, 1 (2023), 107.
- [24] John Weston Hughes, John Theurer, Milos Vukadinovic, Albert J Rogers, Sulaiman Somani, Guson Kang, Zaniar Ghazizadeh, Jack W O'Sullivan, Sneha S Jain, Bruna Gomes, et al. 2025. A deep learning phenome wide association study of the electrocardiogram. *European Heart Journal-Digital Health* (2025), ztaf047.
- [25] Sharifah Noor Masidayu Sayed Ismail, Nor Azlina A Aziz, and Siti Zainab Ibrahim. 2022. A comparison of emotion recognition system using electrocardiogram (ECG) and photoplethysmogram (PPG). *Journal of King Saud University-Computer and Information Sciences* 34, 6 (2022), 3539–3558.
- [26] Hui Jiang, Tianliang Yao, and Cheng Ding. 2025. PPG-based glucose sensors: a review. *Artificial Intelligence Review* 58, 12 (2025), 1–33.
- [27] Alistair EW Johnson, Tom J Pollard, Lu Shen, Li-wei H Lehman, Mengling Feng, Mohammad Ghassemi, Benjamin Moody, Peter Szolovits, Leo Anthony Celi, and Roger G Mark. 2016. MIMIC-III, a freely accessible critical care database. *Scientific data* 3, 1 (2016), 1–9.
- [28] Mohamad Kachuee, Mohammad Kiani, Hoda Mohammadzade, and Mahdi Shabany. 2015. Cuff-Less Blood Pressure Estimation Dataset. UCI Machine Learning Repository. doi:10.24432/C5B602
- [29] Aman Kansal, Emma Chen, Boyang Tom Jin, Pranav Rajpurkar, and David A Kim. 2025. MC-MED, multimodal clinical monitoring in the emergency department. *Scientific Data* 12, 1 (2025), 1094.
- [30] Bojana Koteska, Ana Madevska Bodanova, Hristina Mitrova, Marija Sidorenko, and Fedor Lehocki. 2022. A deep learning approach to estimate SpO₂ from PPG signals. In *Proceedings of the 9th International Conference on Bioinformatics Research and Applications*. 142–148.
- [31] H Lee, H Chung, and J Lee. 2018. Motion artifact cancellation in wearable photoplethysmography using gyroscope. *IEEE Sensors Journal* 19, 3 (2018), 1166–1175.
- [32] Hyung-Chul Lee, Yoosang Park, Soo Bin Yoon, Seong Mi Yang, Dongnyeok Park, and Chul-Woo Jung. 2022. VitalDB, a high-fidelity multi-parameter vital signs database in surgical patients. *Scientific Data* 9, 1 (2022), 279.
- [33] Jun Li, Aaron D Aguirre, Valdey Moura Junior, Jiarui Jin, Che Liu, Lanhai Zhong, Chenxi Sun, Gari Clifford, M Brandon Westover, and Shenda Hong. 2025. An Electrocardiogram Foundation Model Built on over 10 Million Recordings. *NEJM AI* 2, 7 (2025), A1oa2401033.
- [34] Jun Li, Hongling Zhu, Yujie Xiao, Qinghao Zhao, Yalei Ke, Gongzheng Tang, Guangkun Nie, Deyun Zhang, Jin Li, Canqing Yu, et al. 2026. AnyECG: Evolved ECG Foundation Model for Holistic Health Profiling. *arXiv preprint arXiv:2601.10748* (2026).
- [35] Chin Lin, Chin-Sheng Lin, Sy-Jou Chen, Shi-Hung Tsai, Chih-Chien Sung, Chien-Chou Chen, Yu-Juei Hsu, Yi-Jen Hung, and Shih-Hua Lin. 2026. AI-enabled electrocardiogram alert for potassium imbalance treatment: a pragmatic randomized controlled trial. *Nature Communications* 17, 1 (2026), 159.
- [36] Ilya Loshchilov, Frank Hutter, et al. 2017. Fixing weight decay regularization in adam. *arXiv preprint arXiv:1711.05101* 5, 5 (2017), 5.
- [37] Ming Y Lu, Bowen Chen, Drew FK Williamson, Richard J Chen, Melissa Zhao, Aaron K Chow, Kenji Ikemura, Ahron Kim, Dimitra Pouli, Ankush Patel, et al. 2024. A multimodal generative AI copilot for human pathology. *Nature* 634, 8033 (2024), 466–473.
- [38] DongAo Ma, Jiaxuan Pang, Michael B Gotway, and Jianming Liang. 2025. A fully open AI foundation model applied to chest radiography. *Nature* (2025), 1–11.
- [39] Dominique Makowski, Tam Pham, Zen J Lau, Jan C Brammer, François Lespinasse, Hung Pham, Christopher Schölzel, and SH Annabel Chen. 2021. NeuroKit2: A Python toolbox for neurophysiological signal processing. *Behavior research methods* 53, 4 (2021), 1689–1696.
- [40] Andrew C Miller, Joseph Futoma, Salar Abbaspourazad, Christina Heinze-Deml, Saba Emrani, Ian Shapiro, and Guillermo Sapiro. 2025. A wearable-based aging

- clock associates with disease and behavior. *Nature communications* 16, 1 (2025), 9264.
- [41] Seongwook Min, Jaehun An, Jae Hee Lee, Ji Hoon Kim, Daniel J Joe, Soo Hwan Eom, Chang D Yoo, Hyo-Suk Ahn, Jin-Young Hwang, Sheng Xu, et al. 2025. Wearable blood pressure sensors for cardiovascular monitoring and machine learning algorithms for blood pressure estimation. *Nature Reviews Cardiology* (2025), 1–20.
- [42] Mina Namvari, Jessica Lipoth, Sheida Knight, Ali Akbar Jamali, Mojtaba Hedayati, Raymond J Spiteri, and Shabbir Syed-Abdul. 2022. Photoplethysmography enabled wearable devices and stress detection: a scoping review. *Journal of Personalized Medicine* 12, 11 (2022), 1792.
- [43] Andrea Nemcova, Enikő Vargova, Radovan Smisek, Lucie Marsanova, Lukas Smital, and Martin Vitek. 2021. Brno university of technology smartphone ppg database (but ppg): Annotated dataset for ppg quality assessment and heart rate estimation. *BioMed Research International* 2021, 1 (2021), 3453007.
- [44] Guangkun Nie, Xuesong Chen, Yichen Wang, Jingxu Chen, Yunhan Shi, Jianwen Zhong, Weijun Huang, Zengrui Jin, Fei Lei, Leilei Wang, et al. 2025. A Low-Burden Sleep Foundation Model Built on Respiratory and Heartbeat Signals from 780,000+ Hours of Multi-Ethnic Sleep Recordings. *medRxiv* (2025), 2025–09.
- [45] Guangkun Nie, Qinghao Zhao, Gongzheng Tang, Yaxin Li, and Shenda Hong. 2025. Artificial Intelligence-derived Vascular Age from Photoplethysmography: A Novel Digital Biomarker for Cardiovascular Health. *arXiv preprint arXiv:2502.12990* (2025).
- [46] Guangkun Nie, Jiabao Zhu, Gongzheng Tang, Deyun Zhang, Shijia Geng, Qinghao Zhao, and Shenda Hong. 2024. A review of deep learning methods for photoplethysmography data. *arXiv preprint arXiv:2401.12783* (2024).
- [47] Christina Orphanidou. 2017. Signal quality assessment in physiological monitoring: state of the art and practical considerations. (2017).
- [48] Pankaj, Ashish Kumar, Rama Komaragiri, and Manjeet Kumar. 2022. A review on computation methods used in photoplethysmography signal analysis for heart rate estimation. *Archives of Computational Methods in Engineering* 29, 2 (2022), 921–940.
- [49] Madhuri Panwar, Arvind Gautam, Dwaipayan Biswas, and Amit Acharyya. 2020. PP-Net: A deep learning framework for PPG-based blood pressure and heart rate estimation. *IEEE Sensors Journal* 20, 17 (2020), 10000–10011.
- [50] Tania Pereira, Nate Tran, Kais Gadhomi, Michele M Pelter, Duc H Do, Randall J Lee, Rene Colorado, Karl Meisel, and Xiao Hu. 2020. Photoplethysmography based atrial fibrillation detection: a review. *NPJ digital medicine* 3, 1 (2020), 3.
- [51] Arvind Pillai, Dimitris Spathis, Fahim Kawsar, and Mohammad Malekzadeh. [n. d.]. PaPaGei: Open Foundation Models for Optical Physiological Signals. In *The Thirteenth International Conference on Learning Representations*.
- [52] Alec Radford, Jong Wook Kim, Chris Hallacy, Aditya Ramesh, Gabriel Goh, Sandhini Agarwal, Girish Sastry, Amanda Askell, Pamela Mishkin, Jack Clark, et al. 2021. Learning transferable visual models from natural language supervision. In *International conference on machine learning*. PmlR, 8748–8763.
- [53] Olli A Rantula, Jukka A Lipponen, Jari Halonen, Helena Jäntti, Tuomas T Rissanen, Noora S Naukkarinen, Eemu-Samuli Väliäho, Onni E Santala, Jagdeep Sedha, Tero J Martikainen, et al. 2025. Photoplethysmography in recent-onset atrial fibrillation: automatic detection of rhythm change and burden. *European Heart Journal-Digital Health* (2025), ztaf055.
- [54] Susan Redline, Peter V Tishler, Tor D Tosteson, John Williamson, Kenneth Kump, Ilene Browner, Veronica Ferrette, and Patrick Krejci. 1995. The familial aggregation of obstructive sleep apnea. *American journal of respiratory and critical care medicine* 151, 3 (1995), 682–687.
- [55] Attila Reiss, Ina Indlekofer, and Philip Schmidt. 2019. PPG-DaLiA. UCI Machine Learning Repository. doi:10.24432/C53890
- [56] Mithun Saha, Maxwell A Xu, Wanting Mao, Sameer Neupane, James M Rehg, and Santosh Kumar. 2025. Pulse-ppg: An open-source field-trained ppg foundation model for wearable applications across lab and field settings. *Proceedings of the ACM on Interactive, Mobile, Wearable and Ubiquitous Technologies* 9, 3 (2025), 1–35.
- [57] Pritam Sarkar and Ali Etamad. 2021. Cardiogan: Attentive generative adversarial network with dual discriminators for synthesis of ecg from ppg. In *Proceedings of the AAAI Conference on Artificial Intelligence*, Vol. 35. 488–496.
- [58] Oded Schlesinger, Nitai Vigderhouse, Danny Eytan, and Yair Moshe. 2020. Blood pressure estimation from ppg signals using convolutional neural networks and siamese network. In *ICASSP 2020-2020 IEEE international conference on acoustics, speech and signal processing (ICASSP)*. IEEE, 1135–1139.
- [59] Philip Schmidt, Attila Reiss, Robert Duerichen, Claus Marberger, and Kristof Van Laerhoven. 2018. Introducing wesad, a multimodal dataset for wearable stress and affect detection. In *Proceedings of the 20th ACM international conference on multimodal interaction*. 400–408.
- [60] K Selvakumar, E Vinodh Kumar, M Sailesh, Mamtani Varun, Anbu Allan, Nanda Biswajit, Panga Namrata, and Sivaramkrishnan Upasana. 2022. Realtime PPG based respiration rate estimation for remote health monitoring applications. *Biomedical Signal Processing and Control* 77 (2022), 103746.
- [61] Kamal Shah, Anran Wang, Yiwen Chen, Jitender Munjal, Sumeet Chhabra, Anthony Stange, Enxun Wei, Tuan Phan, Tracy Giest, Beszel Hawkins, et al. 2025. Automated loss of pulse detection on a consumer smartwatch. *Nature* (2025), 1–3.
- [62] Md Nazmul Islam Shuzan, Moajjem Hossain Chowdhury, Muhammad EH Chowdhury, Murugappan Murugappan, Enamul Hoque Bhuiyan, Mohamed Arslane Ayari, and Amith Khandakar. 2023. Machine learning-based respiration rate and blood oxygen saturation estimation using photoplethysmogram signals. *Bioengineering* 10, 2 (2023), 167.
- [63] Ali Siam, Fathi Abd El-Samie, Atef Abu Elazm, Nirmeen El-Bahnasawy, and Ghada Elbanby. 2019. Real-World PPG dataset. doi:10.17632/yynb8t9x3d.1
- [64] Douglas A Simonetto, David Rushlow, Kan Liu, Alberto Calleri, Blake A Kassmeyer, Ryan J Lennon, Puru Rattan, Matthew E Bernard, Gagandeep Singh, Mark E Deyo-Svendsen, et al. 2025. Detection of undiagnosed liver cirrhosis via AI-enabled electrocardiogram: a pragmatic, cluster-randomized clinical trial. *Nature Medicine* (2025), 1–8.
- [65] Erica S Spatz, Geoffrey S Ginsburg, John S Rumsfeld, and Mintu P Turakhia. 2024. Wearable digital health technologies for monitoring in cardiovascular medicine. *New England Journal of Medicine* 390, 4 (2024), 346–356.
- [66] Haoqi Sun, Wolfgang Ganglberger, Samaneh Nasiri, Aditya Gupta, Manohar Ghanta, Valdey Moura Junior, Sydney Cash, Katie Stone, Zhiyong Zhang, Gauri Ganjoo, Thijs E Nassi, Ruoqi Wei, Erik-Jan Meulenbrugge, Rhoda Au, Gari Clifford, Lynn Marie Trotti, Dennis Hwang, Emmanuel Mignot, Umakanth Katwa, and M. Brandon Westover. 2023. The Human Sleep Project (version 2.0). doi:10.60508/qjbv-hg78
- [67] Yue Sun, Limei Wang, Gang Li, Weili Lin, and Li Wang. 2025. A foundation model for enhancing magnetic resonance images and downstream segmentation, registration and diagnostic tasks. *Nature Biomedical Engineering* 9, 4 (2025), 521–538.
- [68] Rahul Thapa, Magnus Ruud Kjaer, Bryan He, Ian Covert, Hyatt Moore IV, Umaer Hanif, Gauri Ganjoo, M Brandon Westover, Poul Jennum, Andreas Brink-Kjaer, et al. 2026. A multimodal sleep foundation model for disease prediction. *Nature Medicine* (2026), 1–11.
- [69] Jessica Torres-Soto and Euan A Ashley. 2020. Multi-task deep learning for cardiac rhythm detection in wearable devices. *NPJ digital medicine* 3, 1 (2020), 116.
- [70] Gaetano Valenza, Zoran Matic, and Vincenzo Catrambone. 2025. The brain–heart axis: Integrative cooperation of neural, mechanical and biochemical pathways. *Nature Reviews Cardiology* (2025), 1–14.
- [71] Li Wan, Kechen Liu, Hanan Abdullah Mengash, Nuha Alruwais, Mesfer Al Duhayyim, and K Venkatachalam. 2024. Deep learning-based photoplethysmography biometric authentication for continuous user verification. *Applied Soft Computing* 156 (2024), 111461.
- [72] Haixue Wang, Jianwei Wang, Wei Jing, Shanshan Dai, Deyun Zhang, Shijia Geng, Haijun Wang, and Shenda Hong. 2025. Reliability and validity of a novel single-lead portable electrocardiogram device for pregnant women: a comparative study. *BMC Medical Informatics and Decision Making* 25, 1 (2025), 108.
- [73] Weinan Wang, Pedram Mohseni, Kevin L Kilgore, and Laleh Najafzadeh. 2023. PulseDB: A large, cleaned dataset based on MIMIC-III and VitalDB for benchmarking cuff-less blood pressure estimation methods. *Frontiers in Digital Health* 4 (2023), 1090854.
- [74] Gareth J Williams, Abdulaziz Al-Baraikhan, Frank E Rademakers, Fabio Ciravegna, Frans N van de Vosse, Allan Lawrie, Alexander Rothman, Euan A Ashley, Martin R Wilkins, Patricia V Lawford, et al. 2023. Wearable technology and the cardiovascular system: the future of patient assessment. *The Lancet Digital Health* 5, 7 (2023), e467–e476.
- [75] Hanwen Xu, Naoto Usuyama, Jaspreet Bagga, Sheng Zhang, Rajesh Rao, Tristan Naumann, Cliff Wong, Zelalem Gero, Javier González, Yu Gu, et al. 2024. A whole-slide foundation model for digital pathology from real-world data. *Nature* 630, 8015 (2024), 181–188.
- [76] Jiahui Yu, Zirui Wang, Vijay Vasudevan, Legg Yeung, Mojtaba Seyedhosseini, and Yonghui Wu. 2022. Coca: Contrastive captioners are image-text foundation models. *arXiv preprint arXiv:2205.01917* (2022).
- [77] Xiaoyan Yuan, Wei Wang, Xiaohe Li, Yuanting Zhang, Xiping Hu, and M Jamal Deen. 2024. CATransformer: A cycle-aware transformer for high-fidelity ECG generation from PPG. *IEEE Journal of Biomedical and Health Informatics* (2024).
- [78] Gaobo Zhang, Zhen Mei, Yuan Zhang, Xuesheng Ma, Benny Lo, Dongyi Chen, and Yuanting Zhang. 2020. A noninvasive blood glucose monitoring system based on smartphone PPG signal processing and machine learning. *IEEE Transactions on Industrial Informatics* 16, 11 (2020), 7209–7218.
- [79] Liping Zhang, Anzi Li, Shukai Chen, Wei Ren, and Kim-Kwang Raymond Choo. 2023. A secure, flexible, and PPG-based biometric scheme for healthy IoT using homomorphic random forest. *IEEE Internet of Things Journal* 11, 1 (2023), 612–622.
- [80] Yuwei Zhang, Kumar Ayush, Siyuan Qiao, A Ali Heydari, Girish Narayanswamy, Maxwell A Xu, Ahmed A Metwally, Shawn Xu, Jake Garrison, Xuhai Xu, et al. 2025. SensorLM: Learning the Language of Wearable Sensors. *arXiv preprint arXiv:2506.09108* (2025).
- [81] Zhidong Zhao and Yefei Zhang. 2018. SQI quality evaluation mechanism of single-lead ECG signal based on simple heuristic fusion and fuzzy comprehensive evaluation. *Frontiers in physiology* 9 (2018), 727.

A The AnyPPG Encoder Architecture

The AnyPPG encoder is a one-dimensional convolutional neural network comprising approximately 4.04M parameters. Detailed layer-wise specifications and module definitions are provided in Table A1 and Table A2, respectively. The architecture begins with a stem layer implemented as a Type 3 ConvBlock, which consists of a 3×1 convolution followed by Batch Normalization and Swish activation, mapping the single-channel input to 64 channels. This is followed by a sequence of BasicStage modules that progressively increase the channel dimension from 64 to 512. Each stage is composed of one BasicBlock (Type 1) followed by $(n-1)$ BasicBlocks (Type 2). Internally, both block types employ a three-layer bottleneck structure consisting of a Type 1 ConvBlock (1×1 convolution), a Type 2 ConvBlock (3×1 convolution), and a second Type 1 ConvBlock (1×1 convolution). These internal ConvBlocks utilize a pre-activation design where Batch Normalization, Swish activation, and Dropout ($p = 0.5$) precede the convolution operation. A Squeeze-and-Excitation module with a reduction ratio of 2 is applied after the convolutional sequence in both block types. The BasicBlock (Type 1) is distinguished by the inclusion of a MaxPool1d layer with a kernel size of 2 and stride of 2 at the end of the module to halve the temporal resolution. The network concludes with a global mean pooling layer applied along the temporal dimension, yielding a final 512-dimensional output embedding.

B Dataset Descriptions

B.1 Datasets for Pretraining

MC-MED Dataset. The MC-MED dataset [29] comprises 118,385 adult encounters recorded at the Stanford Adult Emergency Department between 2020 and 2022. It includes continuous recordings of vital signs and physiological waveforms, such as PPG, ECG, and respiratory signals. Additionally, the dataset provides comprehensive clinical metadata, including patient demographics, medical histories, clinical orders, medication prescriptions, laboratory test results, imaging findings, and documented clinical outcomes.

PulseDB Dataset. The PulseDB dataset [73] is a curated benchmark resource designed for evaluating cuffless blood pressure estimation methods. It consists of synchronized 10-second segments of PPG, ECG, and arterial blood pressure (ABP) waveforms from 5,361 subjects, along with demographic metadata such as age. PulseDB comprises two subsets: the MIMIC-III subset ($n=2,423$), which includes recordings from patients admitted to critical care units at Beth Israel Deaconess Medical Center between 2001 and 2012 [27], and the VitalDB subset ($n=2,938$), which contains intraoperative recordings from surgical patients at Seoul National University Hospital, Republic of Korea [32].

MESA Dataset. The MESA dataset [9] is a longitudinal cohort established between 2000 and 2002 to investigate the prevalence and progression of subclinical cardiovascular disease across diverse ethnic populations. Between 2010 and 2012, 2,237 participants underwent a dedicated Sleep Exam, which included overnight polysomnography (PSG) recordings with synchronized channels such as PPG and ECG.

HSP Dataset. The HSP dataset [66] comprises 25,941 PSG recordings collected from approximately 19,492 unique patients at the Massachusetts General Hospital Sleep Laboratory as of April 1, 2023. Each recording includes a standardized set of physiological channels, with a subset featuring synchronized PPG and ECG.

CFS Dataset. The CFS dataset [54] is a longitudinal, family-based cohort designed to investigate the familial aggregation of sleep apnea. Initiated in 1990, the study enrolled 2,284 individuals (46% African American) from 361 families, with participants assessed up to four times over a 16-year follow-up period.

B.2 Datasets for Downstream Evaluation

PPG-DaLiA Dataset. PPG-DaLiA [55] is a multimodal dataset designed for heart rate estimation during daily life activities. It contains synchronized physiological and motion data recorded from 15 subjects performing eight distinct activities: sitting, ascending/descending stairs, table soccer, cycling, driving, lunch break, walking, and working. These activities were selected to introduce varying levels of motion artifacts under realistic conditions. The dataset includes PPG and 3D-accelerometer signals collected from both wrist- and chest-worn devices, alongside concurrent ECG recordings which serve as the ground truth.

UCI-BP Dataset. UCI-BP [28] is a benchmark dataset for cuffless blood pressure estimation, comprising preprocessed and quality-validated recordings derived from the MIMIC-II Waveform Database. The dataset contains synchronized fingertip PPG, Lead II ECG, and invasive arterial blood pressure (ABP, in mmHg) signals sampled at 125 Hz. The invasive ABP measurements serve as reference targets for systolic and diastolic blood pressure regression.

BUT PPG Dataset. The Brno University of Technology Smartphone PPG (BUT PPG) Dataset [43] is a publicly available benchmark specifically curated for signal quality assessment and heart rate estimation on consumer devices. It comprises 3,888 ten-second PPG segments acquired from a gender-balanced cohort of 50 subjects (aged 19-76 years) under varying conditions, including rest and motion. The dataset features smartphone-recorded PPG signals (30 Hz) synchronized with high-resolution single-lead ECG (1,000 Hz) and tri-axial accelerometer data (100 Hz). Comprehensive ground truth is provided via binary signal quality labels and expert-validated heart rates derived from ECG QRS detection, alongside auxiliary physiological metadata such as blood pressure.

Gyro-Acc-PPG Dataset. Gyro-Acc-PPG contains wrist PPG recordings collected using a custom watch-type wearable device equipped with a three-channel PPG sensor, a tri-axial accelerometer, and a gyroscope. Data were acquired from 24 healthy participants (10 male and 14 female; mean age 26.9 ± 4.8 years) during a structured treadmill exercise protocol including rest, walking, and running stages. Synchronized chest ECG signals recorded with a Holter monitor serve as reference measurements for heart rate. PPG signals were sampled at 50 Hz, and ECG, accelerometer, and gyroscope signals were sampled at 125 Hz, 50 Hz, and 50 Hz, respectively.

DeepBeat Dataset. The DeepBeat dataset [69] contains PPG recordings from 132 patients with atrial fibrillation and provides publicly available validation and test splits. In our experiments, the

Table A1: Architecture and parameter summary of AnyPPG. C_{in} and C_{out} denote the input and output channel dimensions. Output shapes are expressed as $[B, C, L]$, where B is the batch size, C the channel dimension, and L the temporal length.

AnyPPG Encoder (Sequential Architecture)	C_{in}	C_{out}	Output Shape $[B, C, L]$	#Parameters
ConvBlock (Type 3)	1	64	$[B, 64, 1250]$	384
BasicStage ₂	64	64	$[B, 64, 625]$	32,064
BasicStage ₂	64	160	$[B, 160, 313]$	156,768
BasicStage ₂	160	160	$[B, 160, 157]$	172,320
BasicStage ₃	160	400	$[B, 400, 79]$	1,413,720
BasicStage ₃	400	400	$[B, 400, 40]$	1,510,200
BasicStage ₁	400	512	$[B, 512, 20]$	758,816
MeanPool1d	512	512	$[B, 512]$	–
Total	1	512	$[B, 512, 20]$	4,044,272

Table A2: Module definitions in AnyPPG. C_{in} and C_{out} denote the input and output channel dimensions, respectively.

Module	Constituent operations (sequential definition)
BasicStage _{n} (C_{in}, C_{out})	BasicBlock (Type 1) (C_{in}, C_{out}) BasicBlock (Type 2) (C_{out}, C_{out}) $\times (n-1)$
BasicBlock (Type 1) (C_{in}, C_{out})	ConvBlock (Type 1) (C_{in}, C_{out}) ConvBlock (Type 2) (C_{out}, C_{out}) ConvBlock (Type 1) (C_{out}, C_{out}) Squeeze and excitation attention (reduction ratio=2) MaxPool1d (kernel = 2, stride = 2)
BasicBlock (Type 2) (C_{in}, C_{out})	ConvBlock (Type 1) (C_{in}, C_{out}) ConvBlock (Type 2) (C_{out}, C_{out}) ConvBlock (Type 1) (C_{out}, C_{out}) Squeeze and excitation attention (reduction ratio=2)
ConvBlock (Type 1) (C_{in}, C_{out})	BatchNorm1d(C_{in}) Swish() Dropout($p=0.5$) Conv1d(C_{in}, C_{out} , kernel_size=1, stride=1, padding=0)
ConvBlock (Type 2) (C_{in}, C_{out})	BatchNorm1d(C_{in}) Swish() Dropout($p=0.5$) Conv1d(C_{in}, C_{out} , kernel_size=3, stride=1, padding=1)
ConvBlock (Type 3) (C_{in}, C_{out})	Conv1d(C_{in}, C_{out} , kernel_size=3, stride=1, padding=1) BatchNorm1d(C_{in}) Swish()

validation split was used for model training and internal validation, while the official test split was reserved as a holdout test set. This protocol ensures strict patient-level separation between training and evaluation and enables fair performance comparison, following prior practice in [33].

WESAD Dataset. The Wearable Stress and Affect Detection (WESAD) dataset [59] is a publicly available multimodal dataset for emotion and stress recognition using wearable sensors. It contains

synchronized physiological and motion recordings from 15 subjects collected during a controlled laboratory study with both chest-worn (RespiBAN) and wrist-worn (Empatica E4) devices. The chest device provides ECG sampled at 700 Hz, while the wrist device records PPG at 64 Hz. In our experiments, we consider four affective states: baseline, stress, amusement, and meditation.

Real-World PPG Dataset. The Real-World PPG dataset [63] is a publicly available dataset collected using an Internet-of-Things-based

sensor platform for PPG acquisition. It contains PPG recordings from 35 healthy participants (aged 10–75 years), with 50 to 60 signal segments collected per subject. Each PPG segment consists of a 6-second recording sampled at 50 Hz, yielding 300 samples per segment. The dataset is provided with predefined training and test splits, comprising 1,374 and 700 PPG segments, respectively.

WenXinWuYang Dataset. The WenXinWuYang dataset [72] comprises physiological recordings collected using a portable device named WenXinWuYang. It includes PPG signals sampled at 25 Hz together with synchronized ECG signals, where pre-developed ECG analysis algorithms provide reference labels for downstream PPG evaluation. The dataset contains 3,345 recordings of 30-second PPG segments, which are further segmented into 10-second intervals, yielding a total of 10,035 PPG segments.

C Additional Metrics for Downstream Tasks

In this section, we report evaluation metrics extending beyond the primary MAE and AUC results presented in the main text. For regression tasks, we provide the Pearson correlation coefficient (r) in Table A3. For classification tasks, we present accuracy and F1-scores in Tables A4 and A5, respectively. Across these diverse metrics, AnyPPG consistently achieves superior performance, further validating the robustness and generalization capabilities conferred by our large-scale, multi-source pretraining strategy and ECG-guided supervision.

D Results for Phenome-Wide Disease Detection

This section presents the detailed results of the phenome-wide disease detection evaluation. Figure A1 displays the top-60 specific disease phenotypes ranked by AUC, excluding non-specific descriptions (e.g., those containing "other"). The visualization shows that while the highest-performing phenotypes are concentrated within the circulatory system, effective detection extends across diverse physiological chapters. Additionally, Table A6 provides the complete list of all 307 phenotypes that achieved an AUC of ≥ 0.70 .

Table A3: Linear-probing r for regression tasks. Best results are in red, second best are underlined. * indicates identical pretraining data to AnyPPG. Abbr.: HR, heart rate; SBP/DBP, systolic/diastolic blood pressure; RR, respiratory rate.

Dataset	Task	SimCLR* ICML'20	BYOL* NIPS'20	MOMENT ICML'24	Chronos-2 ArXiv'25	PulsePPG IMWUT'25	PaPaGEI-S ICLR'25	PaPaGEI-P ICLR'25	AnyPPG (Ours)
PPG-DaLiA	HR	0.76 _[0.74, 0.78]	0.76 _[0.74, 0.78]	0.73 _[0.71, 0.75]	<u>0.75</u> _[0.73, 0.77]	0.72 _[0.70, 0.74]	0.60 _[0.58, 0.63]	0.68 _[0.66, 0.70]	0.76 _[0.74, 0.78]
BUT PPG	HR	0.58 _[0.37, 0.74]	0.35 _[0.07, 0.61]	0.64 _[0.45, 0.77]	<u>0.71</u> _[0.60, 0.79]	0.57 _[0.45, 0.68]	0.45 _[0.28, 0.59]	0.07 _[-0.14, 0.39]	0.79 _[0.71, 0.86]
	SBP	-0.37 _[-0.52, -0.20]	-0.30 _[-0.49, -0.12]	<u>-0.14</u> _[-0.34, 0.04]	-0.20 _[-0.41, 0.03]	-0.32 _[-0.49, -0.12]	-0.17 _[-0.40, 0.02]	-0.19 _[-0.30, -0.07]	0.04 _[-0.20, 0.28]
	DBP	-0.24 _[-0.41, -0.04]	-0.23 _[-0.35, -0.12]	<u>-0.18</u> _[-0.39, 0.06]	0.00 _[-0.21, 0.21]	-0.21 _[-0.41, 0.03]	-0.28 _[-0.48, -0.07]	0.26 _[0.08, 0.43]	<u>0.22</u> _[0.03, 0.40]
Gyro-Acc-PPG	HR	<u>0.74</u> _[0.68, 0.79]	0.73 _[0.66, 0.78]	0.65 _[0.58, 0.72]	0.69 _[0.64, 0.74]	0.68 _[0.62, 0.74]	0.39 _[0.30, 0.47]	0.60 _[0.53, 0.66]	0.76 _[0.70, 0.81]
UCI-BP	SBP	0.52 _[0.51, 0.52]	<u>0.50</u> _[0.49, 0.51]	0.45 _[0.44, 0.46]	0.39 _[0.39, 0.40]	0.45 _[0.45, 0.46]	0.34 _[0.33, 0.35]	0.42 _[0.41, 0.43]	0.52 _[0.51, 0.53]
	DBP	0.44 _[0.43, 0.45]	0.41 _[0.40, 0.41]	0.35 _[0.34, 0.36]	0.30 _[0.29, 0.30]	0.34 _[0.33, 0.34]	0.21 _[0.21, 0.22]	0.31 _[0.30, 0.32]	<u>0.43</u> _[0.42, 0.44]
WenXinWuYang	HR	<u>0.62</u> _[0.58, 0.65]	<u>0.62</u> _[0.59, 0.65]	<u>0.62</u> _[0.58, 0.65]	<u>0.62</u> _[0.58, 0.65]	0.60 _[0.56, 0.63]	0.35 _[0.31, 0.40]	0.52 _[0.48, 0.55]	0.63 _[0.60, 0.67]
	RR	<u>0.13</u> _[0.09, 0.18]	0.12 _[0.08, 0.16]	0.10 _[0.06, 0.14]	0.13 _[0.09, 0.17]	0.08 _[0.04, 0.13]	0.07 _[0.03, 0.11]	0.12 _[0.08, 0.16]	0.17 _[0.13, 0.20]
	Age	0.29 _[0.25, 0.33]	<u>0.31</u> _[0.26, 0.34]	0.26 _[0.22, 0.30]	0.26 _[0.22, 0.30]	0.23 _[0.18, 0.27]	0.12 _[0.08, 0.17]	0.21 _[0.17, 0.25]	0.33 _[0.29, 0.36]

Table A4: Linear-probing ACC for classification downstream tasks. Best results are in red, second best are underlined. * indicates identical pretraining data to AnyPPG.

Dataset	Task	SimCLR* ICML'20	BYOL* NIPS'20	MOMENT ICML'24	Chronos-2 ArXiv'25	PulsePPG IMWUT'25	PaPaGEI-S ICLR'25	PaPaGEI-P ICLR'25	AnyPPG (Ours)
WESAD	Emotion recognition	0.62 _[0.58, 0.65]	0.57 _[0.54, 0.60]	0.54 _[0.51, 0.57]	0.55 _[0.52, 0.58]	0.56 _[0.53, 0.59]	0.47 _[0.44, 0.51]	0.54 _[0.51, 0.57]	<u>0.61</u> _[0.58, 0.64]
DeepBeat	Atrial fibrillation detection	0.77 _[0.77, 0.78]	<u>0.76</u> _[0.76, 0.77]	<u>0.76</u> _[0.75, 0.76]	<u>0.76</u> _[0.75, 0.76]	0.75 _[0.75, 0.76]	<u>0.76</u> _[0.75, 0.77]	<u>0.76</u> _[0.75, 0.76]	<u>0.76</u> _[0.76, 0.77]
BUT PPG	Signal quality assessment	0.86 _[0.83, 0.88]	0.86 _[0.84, 0.89]	0.86 _[0.84, 0.89]	0.86 _[0.84, 0.89]	0.86 _[0.83, 0.88]	0.86 _[0.83, 0.89]	<u>0.87</u> _[0.84, 0.89]	0.88 _[0.85, 0.90]
Real-World PPG	Biometric identification	0.98 _[0.97, 0.99]	<u>0.93</u> _[0.91, 0.95]	0.61 _[0.57, 0.64]	0.37 _[0.33, 0.40]	0.89 _[0.87, 0.91]	0.33 _[0.29, 0.36]	0.84 _[0.81, 0.86]	0.98 _[0.97, 0.99]
WenXinWuYang	Anomaly detection	0.79 _[0.78, 0.81]	0.80 _[0.79, 0.82]	0.80 _[0.79, 0.82]	<u>0.81</u> _[0.79, 0.82]	0.80 _[0.79, 0.82]	0.77 _[0.76, 0.79]	0.80 _[0.78, 0.82]	0.83 _[0.81, 0.84]

Table A5: Linear-probing F1-score for classification downstream tasks. Best results are in red, second best are underlined. * indicates identical pretraining data to AnyPPG.

Dataset	Task	SimCLR* ICML'20	BYOL* NIPS'20	MOMENT ICML'24	Chronos-2 ArXiv'25	PulsePPG IMWUT'25	PaPaGEI-S ICLR'25	PaPaGEI-P ICLR'25	AnyPPG (Ours)
WESAD	Emotion recognition	0.51 _[0.48, 0.54]	0.47 _[0.44, 0.49]	0.43 _[0.41, 0.46]	0.44 _[0.42, 0.47]	0.44 _[0.42, 0.47]	0.37 _[0.35, 0.40]	0.42 _[0.40, 0.45]	<u>0.50</u> _[0.48, 0.53]
DeepBeat	Atrial fibrillation detection	<u>0.55</u> _[0.54, 0.56]	0.52 _[0.51, 0.53]	0.51 _[0.50, 0.51]	0.57 _[0.56, 0.58]	0.47 _[0.46, 0.47]	0.43 _[0.43, 0.43]	0.43 _[0.43, 0.44]	0.57 _[0.56, 0.58]
BUT PPG	Signal quality assessment	0.59 _[0.54, 0.64]	0.59 _[0.54, 0.64]	<u>0.60</u> _[0.55, 0.66]	0.59 _[0.54, 0.64]	0.55 _[0.51, 0.60]	0.54 _[0.50, 0.59]	0.59 _[0.54, 0.64]	0.67 _[0.62, 0.73]
Real-World PPG	Biometric identification	0.97 _[0.96, 0.99]	<u>0.92</u> _[0.90, 0.94]	0.57 _[0.53, 0.61]	0.34 _[0.30, 0.37]	0.88 _[0.85, 0.90]	0.29 _[0.26, 0.32]	0.82 _[0.79, 0.84]	0.97 _[0.96, 0.99]
WenXinWuYang	Anomaly detection	0.57 _[0.54, 0.59]	0.58 _[0.55, 0.61]	<u>0.61</u> _[0.58, 0.63]	0.60 _[0.57, 0.63]	<u>0.61</u> _[0.59, 0.64]	0.44 _[0.43, 0.44]	0.59 _[0.56, 0.61]	0.67 _[0.65, 0.70]

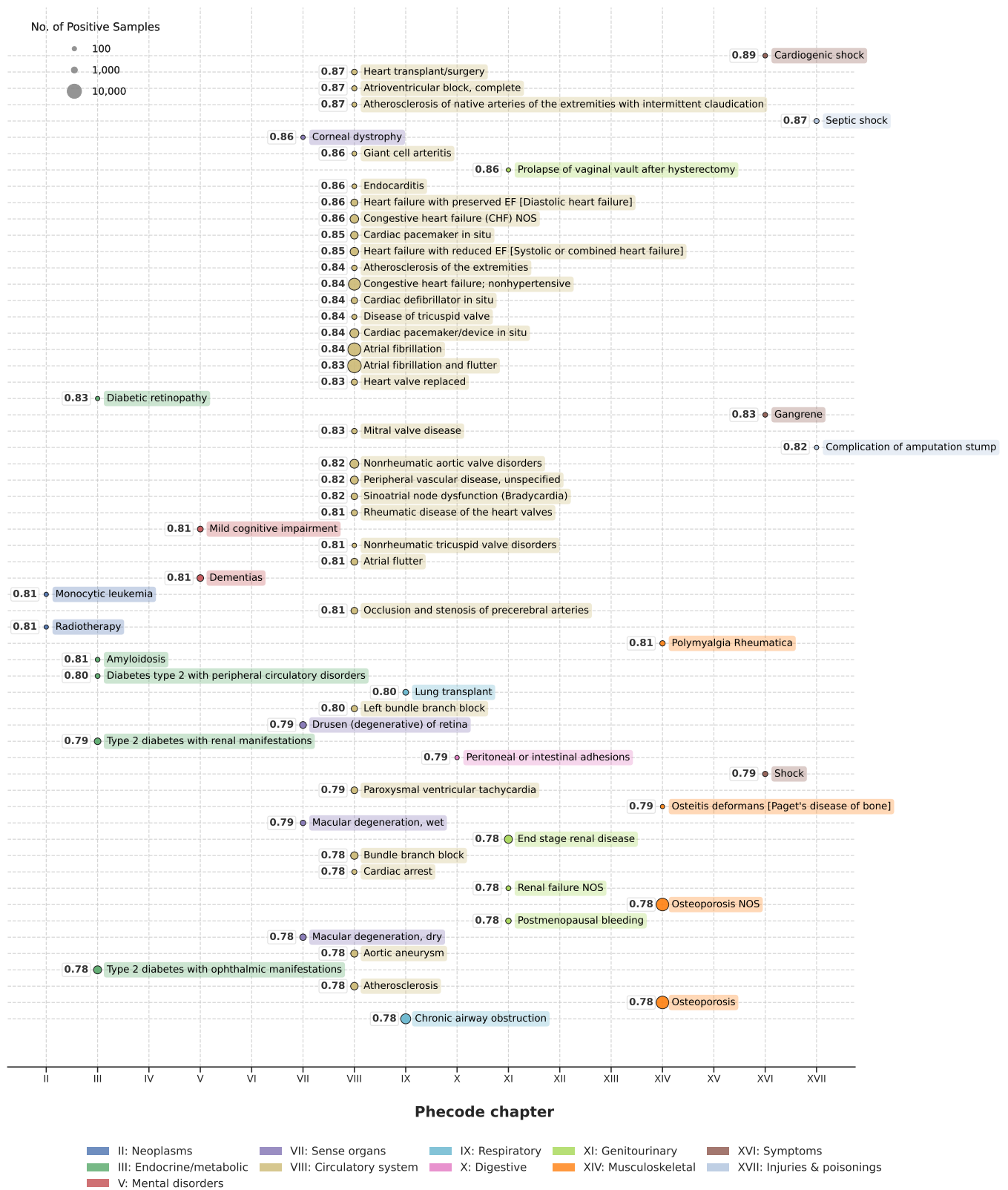


Figure A1: The top 60 disease phenotypes with the highest discriminative performance, ranked by AUC.

Table A6: Detailed phenome-wide disease detection results. N_{pos} and N_{neg} denote the number of positive and negative samples, respectively. AUC values indicate the area under the ROC curve.

Phecode	Description	N_{pos}	N_{neg}	AUC
Chapter I: Infectious diseases				
38.1	Gram negative septicemia	280	359,620	0.74
41.2	Streptococcus infection	360	359,540	0.73
38	Septicemia	6,920	352,980	0.72
117.4	Aspergillosis	180	359,720	0.72
41.12	Methicillin resistant Staphylococcus aureus	640	359,260	0.70
Chapter II: Neoplasms				
196	Radiotherapy	100	359,800	0.81
204.3	Monocytic leukemia	100	359,800	0.81
189.4	Malignant neoplasm of other urinary organs	360	359,540	0.79
172.22	Squamous cell carcinoma	1,320	358,580	0.77
172.3	Carcinoma in situ of skin	560	359,340	0.75
189.2	Cancer of bladder	1,200	358,700	0.75
198.6	Secondary malignancy of bone	2,140	357,760	0.75
198.2	Secondary malignancy of respiratory organs	780	359,120	0.74
155	Cancer of liver and intrahepatic bile duct	1,460	358,440	0.73
165	Cancer within the respiratory system	2,100	357,800	0.73
165.1	Cancer of bronchus; lung	2,080	357,820	0.73
172.2	Other non-epithelial cancer of skin	6,040	353,860	0.73
189.21	Malignant neoplasm of bladder	1,100	358,800	0.73
195	Cancer, suspected or other	4,100	355,800	0.73
202.22	Reticulosarcoma	1,020	358,880	0.73
204.21	Myeloid leukemia, acute	560	359,340	0.73
155.1	Malignant neoplasm of liver, primary	1,060	358,840	0.72
159.2	Malignant neoplasm of small intestine, including duodenum	200	359,700	0.72
159.3	Malignant neoplasm of gallbladder and extrahepatic bile ducts	240	359,660	0.72
172	Skin cancer	7,600	352,300	0.72
172.21	Basal cell carcinoma	3,300	356,600	0.72
174.1	Breast cancer [female]	7,060	352,840	0.72
182	Malignant neoplasm of uterus	1,200	358,700	0.72
185	Cancer of prostate	3,640	356,260	0.72
189	Cancer of urinary organs (incl. kidney and bladder)	2,480	357,420	0.72
198	Secondary malignant neoplasm	5,580	354,320	0.72
198.5	Secondary malignancy of brain/spine	1,040	358,860	0.72
149.1	Cancer of oropharynx	380	359,520	0.71
149.4	Cancer of larynx	160	359,740	0.71
159	Malignant neoplasm of other and ill-defined sites within the digestive organs and peritoneum	900	359,000	0.71
172.1	Melanomas of skin, dx or hx	3,700	356,200	0.71
174	Breast cancer	7,140	352,760	0.71
174.11	Malignant neoplasm of female breast	6,460	353,440	0.71
184.1	Malignant neoplasm of ovary and other uterine adnexa	1,060	358,840	0.71
195.1	Malignant neoplasm, other	2,060	357,840	0.71
204.4	Multiple myeloma	940	358,960	0.71
151	Cancer of stomach	560	359,340	0.70
184	Cancer of other female genital organs	1,660	358,240	0.70
204.2	Myeloid leukemia	920	358,980	0.70
Chapter III: Endocrine/metabolic				
250.7	Diabetic retinopathy	100	359,800	0.83
270.33	Amyloidosis	300	359,600	0.81
250.25	Diabetes type 2 with peripheral circulatory disorders	380	359,520	0.80
250.22	Type 2 diabetes with renal manifestations	1,480	358,420	0.79
250.23	Type 2 diabetes with ophthalmic manifestations	2,600	357,300	0.78
250.11	Type 1 diabetes with ketoacidosis	240	359,660	0.77
270.32	Paraproteinemia	720	359,180	0.77
260.3	Adult failure to thrive	1,740	358,160	0.76

Continued on next page

Table A6 continued from previous page

Phcode	Description	N_{pos}	N_{neg}	AUC
253.7	Other disorders of neurohypophysis	180	359,720	0.75
276.13	Hyperpotassemia	1,620	358,280	0.75
274.2	Crystal arthropathies	280	359,620	0.74
276.6	Fluid overload	1,180	358,720	0.74
274.21	Chondrocalcinosis	280	359,620	0.73
275.3	Disorders of magnesium metabolism	1,000	358,900	0.73
250.2	Type 2 diabetes	23,580	336,320	0.72
250.24	Type 2 diabetes with neurological manifestations	1,660	358,240	0.72
255.12	Hyperaldosteronism	120	359,780	0.72
270.11	Disturbances of sulphur-bearing amino-acid metabolism	200	359,700	0.72
276.11	Hyperosmolality and/or hypernatremia	200	359,700	0.72
249	Secondary diabetes mellitus	740	359,160	0.71
250	Diabetes mellitus	31,380	328,520	0.71
250.3	Insulin pump user	1,600	358,300	0.71
275.6	Hypercalcemia	1,320	358,580	0.71
276.12	Hyposmolality and/or hyponatremia	5,580	354,320	0.71
276.4	Acid-base balance disorder	1,680	358,220	0.71
251.1	Hypoglycemia	740	359,160	0.70
276.41	Acidosis	1,640	358,260	0.70
Chapter IV: Hematopoietic				
285.21	Anemia in chronic kidney disease	1,260	358,640	0.75
286.2	Encounter for long-term (current) use of anticoagulants	3,760	356,140	0.75
286.9	Abnormal coagulation profile	400	359,500	0.74
285.2	Anemia of chronic disease	2,220	357,680	0.72
281.12	Other vitamin B12 deficiency anemia	480	359,420	0.71
286.6	Defibrination syndrome	160	359,740	0.71
Chapter V: Mental disorders				
290.1	Dementias	1,480	358,420	0.81
292.2	Mild cognitive impairment	900	359,000	0.81
315.3	Intellectual disability	180	359,720	0.77
290.11	Alzheimer's disease	140	359,760	0.76
290	Delirium dementia and amnesic and other cognitive disorders	2,600	357,300	0.75
292.11	Aphasia	600	359,300	0.72
292.4	Altered mental status	5,000	354,900	0.71
292.3	Memory loss	2,400	357,500	0.70
Chapter VI: Neurological				
332	Parkinson's disease	1,300	358,600	0.77
350.5	Abnormal reflex	160	359,740	0.74
327.5	Parasomnia	360	359,540	0.73
350.2	Abnormality of gait	7,780	352,120	0.71
359.2	Myopathy	260	359,640	0.71
333.1	Essential tremor	780	359,120	0.70
356	Hereditary and idiopathic peripheral neuropathy	560	359,340	0.70
Chapter VII: Sense organs				
364.5	Corneal dystrophy	120	359,780	0.86
362.22	Macular degeneration, wet	680	359,220	0.79
362.27	Drusen (degenerative) of retina	1,560	358,340	0.79
362.21	Macular degeneration, dry	1,320	358,580	0.78
362.2	Degeneration of macula and posterior pole of retina	5,840	354,060	0.77
362.29	Macular degeneration (senile) of retina NOS	640	359,260	0.77
366	Cataract	17,760	342,140	0.77
362.26	Macular puckering of retina	2,540	357,360	0.76
365.1	Open-angle glaucoma	1,920	357,980	0.75
365.11	Primary open angle glaucoma	1,400	358,500	0.75
366.2	Senile cataract	11,200	348,700	0.75
374.6	Dermatochalasis	1,020	358,880	0.75
374.1	Ectropion or entropion	380	359,520	0.74

Continued on next page

Table A6 continued from previous page

Phcode	Description	N_{pos}	N_{neg}	AUC
389.1	Sensorineural hearing loss	4,540	355,360	0.74
365.2	Primary angle-closure glaucoma	1,700	358,200	0.73
362	Other retinal disorders	9,280	350,620	0.72
362.23	Cystoid macular degeneration of retina	1,300	358,600	0.72
364.2	Corneal edema	180	359,720	0.72
365	Glaucoma	8,360	351,540	0.72
367.4	Presbyopia	4,200	355,700	0.72
379.5	Disorders of iris and ciliary body	340	359,560	0.72
389.3	Degenerative and vascular disorders of ear	520	359,380	0.72
375	Disorders of lacrimal system	4,820	355,080	0.71
375.1	Dry eyes	4,500	355,400	0.71
389.5	Disorders of acoustic nerve	160	359,740	0.70
Chapter VIII: Circulatory system				
429.1	Heart transplant/surgery	800	359,100	0.87
426.24	Atrioventricular block, complete	520	359,380	0.87
440.22	Atherosclerosis of native arteries of the extremities with intermittent claudication	300	359,600	0.87
446.5	Giant cell arteritis	260	359,640	0.86
420.3	Endocarditis	280	359,620	0.86
428.4	Heart failure with preserved EF [Diastolic heart failure]	1,740	358,160	0.86
428.1	Congestive heart failure (CHF) NOS	3,040	356,860	0.86
426.91	Cardiac pacemaker in situ	2,120	357,780	0.85
428.3	Heart failure with reduced EF [Systolic or combined heart failure]	2,880	357,020	0.85
440.2	Atherosclerosis of the extremities	640	359,260	0.84
428	Congestive heart failure; nonhypertensive	6,700	353,200	0.84
426.92	Cardiac defibrillator in situ	1,220	358,680	0.84
394.7	Disease of tricuspid valve	440	359,460	0.84
426.9	Cardiac pacemaker/device in situ	3,440	356,460	0.84
411.8	Other chronic ischemic heart disease, unspecified	480	359,420	0.84
427.21	Atrial fibrillation	8,340	351,560	0.84
427.2	Atrial fibrillation and flutter	9,260	350,640	0.83
395.6	Heart valve replaced	1,100	358,800	0.83
425.8	Other cardiomyopathy	200	359,700	0.83
394.2	Mitral valve disease	700	359,200	0.83
395.2	Nonrheumatic aortic valve disorders	3,360	356,540	0.82
443.9	Peripheral vascular disease, unspecified	2,520	357,380	0.82
427.8	Sinoatrial node dysfunction (Bradycardia)	1,340	358,560	0.82
394	Rheumatic disease of the heart valves	1,080	358,820	0.81
395.3	Nonrheumatic tricuspid valve disorders	140	359,760	0.81
427.22	Atrial flutter	1,680	358,220	0.81
433.1	Occlusion and stenosis of precerebral arteries	1,520	358,380	0.81
426.32	Left bundle branch block	1,180	358,720	0.80
427.12	Paroxysmal ventricular tachycardia	1,520	358,380	0.79
426.3	Bundle branch block	2,080	357,820	0.78
427.42	Cardiac arrest	440	359,460	0.78
442.1	Aortic aneurysm	1,900	358,000	0.78
440	Atherosclerosis	2,120	357,780	0.78
427.4	Cardiac arrest and ventricular fibrillation	500	359,400	0.78
395	Heart valve disorders	6,520	353,380	0.78
426.2	Atrioventricular [AV] block	1,240	358,660	0.77
428.2	Heart failure NOS	400	359,500	0.77
433.11	Occlusion of cerebral arteries, with cerebral infarction	160	359,740	0.76
411.4	Coronary atherosclerosis	9,760	350,140	0.76
426	Cardiac conduction disorders	7,380	352,520	0.76
425	Cardiomyopathy	3,440	356,460	0.76
440.1	Atherosclerosis of renal artery	240	359,660	0.76
411	Ischemic Heart Disease	12,520	347,380	0.76
411.1	Unstable angina (intermediate coronary syndrome)	540	359,360	0.75
425.1	Primary/intrinsic cardiomyopathies	3,120	356,780	0.75

Continued on next page

Table A6 continued from previous page

Phcode	Description	N_{pos}	N_{neg}	AUC
411.2	Myocardial infarction	4,060	355,840	0.75
457.2	Encounter for long-term (current) use of antiplatelets/antithrombotics	760	359,140	0.75
443	Peripheral vascular disease	3,860	356,040	0.75
442.3	Aneurysm of artery of lower extremity	100	359,800	0.75
433.21	Cerebral artery occlusion, with cerebral infarction	4,480	355,420	0.75
433.2	Occlusion of cerebral arteries	4,500	355,400	0.75
442.11	Abdominal aortic aneurysm	600	359,300	0.74
457	Encounter for long-term (current) use of anticoagulants, antithrombotics, aspirin	900	359,000	0.74
433	Cerebrovascular disease	10,000	349,900	0.74
433.3	Cerebral ischemia	3,940	355,960	0.74
411.9	Other acute and subacute forms of ischemic heart disease	440	359,460	0.74
401	Hypertension	46,820	313,080	0.74
440.9	Atherosclerosis of aorta	1,120	358,780	0.73
429.2	Abnormal function study of cardiovascular system	340	359,560	0.73
426.23	Second degree AV block	260	359,640	0.73
401.1	Essential hypertension	46,240	313,660	0.73
433.31	Transient cerebral ischemia	3,700	356,200	0.73
447.1	Stricture of artery	100	359,800	0.73
401.3	Other hypertensive complications	1,120	358,780	0.73
442	Other aneurysm	3,040	356,860	0.73
416	Cardiomegaly	1,200	358,700	0.73
426.31	Right bundle branch block	820	359,080	0.73
401.2	Hypertensive heart and/or renal disease	880	359,020	0.73
425.12	Other hypertrophic cardiomyopathy	500	359,400	0.73
414	Other forms of chronic heart disease	840	359,060	0.72
415.2	Chronic pulmonary heart disease	2,240	357,660	0.72
459.9	Circulatory disease NEC	3,320	356,580	0.72
411.3	Angina pectoris	1,560	358,340	0.72
395.1	Nonrheumatic mitral valve disorders	3,200	356,700	0.72
425.2	Secondary/extrinsic cardiomyopathies	180	359,720	0.71
447	Other disorders of arteries and arterioles	1,880	358,020	0.71
458.9	Hypotension NOS	1,800	358,100	0.70
Chapter IX: Respiratory				
505	Other pulmonary inflammation or edema	520	359,380	0.80
510.2	Lung transplant	880	359,020	0.80
496	Chronic airway obstruction	4,520	355,380	0.78
501	Pneumonitis due to inhalation of food or vomitus	1,040	358,860	0.78
510	Other diseases of lung	1,420	358,480	0.78
504.1	Idiopathic fibrosing alveolitis	220	359,680	0.77
496.1	Emphysema	580	359,320	0.76
503	Pulmonary congestion and hypostasis	100	359,800	0.76
504	Other alveolar and parietoalveolar pneumonopathy	1,040	358,860	0.76
496.2	Chronic bronchitis	1,180	358,720	0.75
509.1	Respiratory failure	3,100	356,800	0.75
496.21	Obstructive chronic bronchitis	840	359,060	0.74
496.3	Bronchiectasis	960	358,940	0.74
480.5	Bronchopneumonia and lung abscess	160	359,740	0.73
502	Postinflammatory pulmonary fibrosis	400	359,500	0.73
480.1	Bacterial pneumonia	900	359,000	0.72
480	Pneumonia	7,000	352,900	0.71
507	Pleurisy; pleural effusion	2,480	357,420	0.71
509	Respiratory failure, insufficiency, arrest	5,940	353,960	0.71
480.11	Pneumococcal pneumonia	220	359,680	0.70
500.1	Extrinsic allergic alveolitis	160	359,740	0.70
509.2	Respiratory insufficiency	440	359,460	0.70
Chapter X: Digestive				
556	Ulceration of the lower GI tract	180	359,720	0.75
556.1	Ulceration of intestine	160	359,740	0.74

Continued on next page

Table A6 continued from previous page

Phcode	Description	N_{pos}	N_{neg}	AUC
560.3	Peritoneal or intestinal adhesions	100	359,800	0.79
562.1	Diverticulosis	3,440	356,460	0.71
565.1	Anal and rectal polyp	120	359,780	0.71
571.81	Portal hypertension	960	358,940	0.71
573.4	Acute and subacute necrosis of liver	400	359,500	0.70
Chapter XI: Genitourinary				
618.5	Prolapse of vaginal vault after hysterectomy	100	359,800	0.86
585.2	Renal failure NOS	360	359,540	0.78
585.32	End stage renal disease	2,660	357,240	0.78
627.1	Postmenopausal bleeding	760	359,140	0.78
585.3	Chronic renal failure [CKD]	6,840	353,060	0.75
618.1	Prolapse of vaginal walls	1,620	358,280	0.75
580.2	Nephrotic syndrome without mention of glomerulonephritis	540	359,360	0.74
585.31	Renal dialysis	1,720	358,180	0.74
585.34	Chronic Kidney Disease, Stage IV	1,500	358,400	0.74
588	Disorders resulting from impaired renal function	1,180	358,720	0.74
588.2	Secondary hyperparathyroidism (of renal origin)	1,120	358,780	0.74
600	Hyperplasia of prostate	5,960	353,940	0.74
627.3	Postmenopausal atrophic vaginitis	1,260	358,640	0.74
585	Renal failure	14,680	345,220	0.73
618	Genital prolapse	2,220	357,680	0.73
627	Menopausal and postmenopausal disorders	3,880	356,020	0.72
585.1	Acute renal failure	8,840	351,060	0.71
585.4	Chronic kidney disease, Stage I or II	1,100	358,800	0.71
587	Kidney replaced by transplant	2,360	357,540	0.71
599.6	Oliguria and anuria	140	359,760	0.71
611.1	Abnormal mammogram	1,600	358,300	0.71
627.2	Symptomatic menopause	1,520	358,380	0.71
586.2	Cyst of kidney, acquired	1,120	358,780	0.70
599.4	Urinary incontinence	3,860	356,040	0.70
618.2	Uterine/Uterovaginal prolapse	880	359,020	0.70
796	Elevated prostate specific antigen [PSA]	1,940	357,960	0.70
Chapter XII: Pregnancy complications				
653	Problems associated with amniotic cavity and membranes	1,180	358,720	0.74
635.2	Antepartum hemorrhage, abruptio placentae, and placenta previa	2,360	357,540	0.72
647	Infectious and parasitic complications affecting pregnancy	600	359,300	0.72
635	Hemorrhage during pregnancy; childbirth and postpartum	2,600	357,300	0.71
636	Early or threatened labor; hemorrhage in early pregnancy	4,560	355,340	0.71
636.3	Hemorrhage in early pregnancy	4,320	355,580	0.71
643	Excessive vomiting in pregnancy	2,060	357,840	0.71
635.3	Placenta previa and abruptio placenta	280	359,620	0.70
Chapter XIII: Dermatologic				
701.1	Keratoderma, acquired	140	359,760	0.78
702.4	Degenerative skin disorders	120	359,780	0.78
707.2	Chronic ulcer of leg or foot	2,060	357,840	0.77
702.1	Actinic keratosis	1,860	358,040	0.75
707	Chronic ulcer of skin	3,220	356,680	0.73
938.2	Chronic dermatitis due to solar radiation	280	359,620	0.73
687.3	Changes in skin texture	120	359,780	0.72
702	Degenerative skin conditions and other dermatoses	2,640	357,260	0.72
707.1	Decubitus ulcer	860	359,040	0.72
709.3	Systemic sclerosis	260	359,640	0.72
709.6	Other specified diffuse diseases of connective tissue	200	359,700	0.70
Chapter XIV: Musculoskeletal				
717	Polymyalgia Rheumatica	640	359,260	0.81
731.1	Osteitis deformans [Paget's disease of bone]	100	359,800	0.79
743.1	Osteoporosis	7,700	352,200	0.78

Continued on next page

Table A6 continued from previous page

Phecode	Description	N_{pos}	N_{neg}	AUC
743.11	Osteoporosis NOS	7,700	352,200	0.78
740.2	Osteoarthritis, generalized	440	359,460	0.76
743	Osteoporosis, osteopenia and pathological fracture	9,000	350,900	0.76
737.1	Kyphosis (acquired)	260	359,640	0.74
710	Osteomyelitis, periostitis, and other infections involving bone	2,460	357,440	0.73
710.1	Osteomyelitis	2,460	357,440	0.73
710.11	Acute osteomyelitis	480	359,420	0.73
710.19	Unspecified osteomyelitis	1,980	357,920	0.73
720.1	Spinal stenosis of lumbar region	3,960	355,940	0.73
740	Osteoarthritis	14,640	345,260	0.73
740.11	Osteoarthritis, localized, primary	10,360	349,540	0.73
740.9	Osteoarthritis NOS	4,720	355,180	0.73
727.5	Rupture of synovium	560	359,340	0.72
740.1	Osteoarthritis; localized	11,100	348,800	0.72
720	Spinal stenosis	6,100	353,800	0.71
735.21	Hammer toe (acquired)	300	359,600	0.71
739	Contracture of joint	440	359,460	0.71
721.2	Spondylosis with myelopathy	540	359,360	0.70
731	Osteitis deformans and osteopathies associated with other disorders classified elsewhere	180	359,720	0.70
735.2	Acquired toe deformities	620	359,280	0.70
Chapter XVI: Symptoms				
797.1	Cardiogenic shock	260	359,640	0.89
791	Gangrene	300	359,600	0.83
797	Shock	580	359,320	0.79
795.8	Abnormal tumor markers	120	359,780	0.75
772.3	Muscle weakness	2,240	357,660	0.70
Chapter XVII: Injuries & poisonings				
994.21	Septic shock	480	359,420	0.87
874	Complication of amputation stump	100	359,800	0.82
961	Poisoning by other anti-infectives	120	359,780	0.81
854	Complications of cardiac/vascular device, implant, and graft	1,220	358,680	0.76
800.1	Fracture of neck of femur	1,580	358,320	0.75
972	Poisoning by agents primarily affecting the cardiovascular system	100	359,800	0.72
994.2	Sepsis	5,660	354,240	0.72
851	Complications of transplants and reattached limbs	2,000	357,900	0.71
994	Sepsis and SIRS	6,020	353,880	0.71
816	Cerebral laceration and contusion	120	359,780	0.70
858	Complication of internal orthopedic device	1,560	358,340	0.70